horticulturae

MDPI

Article

Genome-Wide Identification of *AGO*, *DCL*, and *RDR* Genes and Their Expression Analysis in Response to Drought Stress in Peach

Mohammad Belal [1,2,3,4], Charmaine Ntini [1,2], Cherono Sylvia [1,2], Misganaw Wassie [2,5], Mahmoud Magdy [6,7], Collins Ogutu [8], Mohamed Ezzat [1,2,3], Md Dulal Ali Mollah [1,2], Yunpeng Cao [1,2], Weihan Zhang [1,9], Elsayed Nishawy [1,3,*] and Yuepeng Han [1,2,9,*]

1 CAS Key Laboratory of Plant Germplasm Enhancement and Specialty Agriculture, Wuhan Botanical Garden, The Innovative Academy of Seed Design of Chinese Academy of Sciences, Wuhan 430074, China; maabdrc@mails.ucas.ac.cn (M.B.); charmy1ntini@mails.ucas.ac.cn (C.N.); cherono57@wbgcas.cn (C.S.); dr_mohamed201110@mails.ucas.ac.cn (M.E.); dulal_hort@ru.ac.bd (M.D.A.M.); caoyunpeng@wbgcas.cn (Y.C.); whzhang@wbgcas.cn (W.Z.)
2 University of Chinese Academy of Sciences, 19A Yuquanlu, Beijing 100049, China; misgie2010@yahoo.com
3 Laboratory of Genomics and Genome Editing, Genetic Resources Department, Desert Research Center, Cairo 11753, Egypt
4 Fruit Unit, Department of Plant Production, Ecology and Dry Lands Agriculture Division, Desert Research Center, Cairo 11753, Egypt
5 Xishuangbanna Tropical Botanical Garden, Chinese Academy of Sciences, Kunming 666300, China
6 Department of Plant Biology, Faculty of Biology, Murcia University, 30100 Murcia, Spain; m.elmosallamy@agr.asu.edu.eg
7 Genetics Department, Faculty of Agriculture, Ain Shams University, Cairo 11241, Egypt
8 Fraunhofer Institute for Process Engineering and Packaging, IVV, 85354 Freising, Germany; collee52@gmail.com
9 Sino-African Joint Research Center, Chinese Academy of Sciences, Wuhan 430074, China
* Correspondence: elnishawy@yahoo.com (E.N.); yphan@wbgcas.cn (Y.H.)

Citation: Belal, M.; Ntini, C.; Sylvia, C.; Wassie, M.; Magdy, M.; Ogutu, C.; Ezzat, M.; Mollah, M.D.A.; Cao, Y.; Zhang, W.; et al. Genome-Wide Identification of *AGO*, *DCL*, and *RDR* Genes and Their Expression Analysis in Response to Drought Stress in Peach. *Horticulturae* **2024**, *10*, 1228. https://doi.org/10.3390/horticulturae10111228

Academic Editor: Qiang-Sheng Wu

Received: 29 September 2024
Revised: 1 November 2024
Accepted: 11 November 2024
Published: 20 November 2024

Abstract: Small RNAs (sRNAs) control a wide range of development and physiological pathways in plants. To address the response of sRNA biogenesis to drought stress, we identified sRNA biogenesis genes, including 11 encoding argonautes (AGO), 8 encoding Dicer-like proteins (DCL), and 9 encoding RNA-dependent RNA polymerases (RDR) in the peach genome. Notably, the largest numbers of sRNA biogenesis genes are located to chromosome 1. The PAZ, PIWI, and MID domains were identified in PpAGOs, while the ribonuclease IIIa and IIIb domains were characterized in PpDCLs. The RDRP domain was recognized in PpRDRs. Orthologous similarity and collinearity analyses between Arabidopsis and peach revealed 5, 1, and 2 collinear blocks in AGOs, DCLs, and RDRs, respectively. Moreover, 41, 40, and 42 *cis*-acting elements were located in the promoters of *PpAGOs*, *PpDCLs*, and *PpRDRs*, respectively, with the majority related to drought stress response. Analysis of RNA sequencing (RNA-seq) data revealed that sRNA biogenesis genes were involved in drought stress response in different tissues. Furthermore, the expression of candidate genes was verified in two peach cultivars, Beijing 2-7 (BJ2-7) and Sinai (SN), which are tested as drought-tolerant and sensitive cultivars, respectively, based on the physiological and biochemical analyses, which revealed that the Chinese peach cultivar 'BJ2-7' exhibits greater drought resistance compared to the Egyptian peach cultivar 'SN'. Interestingly, the expression of *PpAGO2b*, *PpDCL2b*, *PpDCL4*, and *PpRDR4* genes was induced in 'BJ2-7' but inhibited in 'SN' under drought stress. Overall, this study provides insight into the roles of sRNA biogenesis genes in response to drought stress in peach.

Keywords: *Prunus persica*; drought; small RNAs; *AGO*; *DCL*; *RDR*; genome-wide identification; gene expression

1. Introduction

Peach (*Prunus persica* L.) is one of the most economically important fruit crops in the Rosaceae family, cultivated worldwide [1,2]. Recently, peach has become an emerging model species for fruit crop genomics studies due to its short life cycle compared to a large scale of fruit trees (maturity in 3–5 years, living around 12 years) and small genome size [3,4]. However, the growth, development, and productivity of peaches are adversely affected by environmental factors, including drought stress [5,6]. During drought stress, plants develop complex and interconnected drought tolerance mechanisms at morphological, physiological, biochemical, and molecular levels [7,8]. Several signaling pathways are activated to mediate the expression of drought stress–related genes. Studies have dissected the underlying mechanisms that influence the transcriptional and post-transcriptional regulation of drought stress response in plants [9]. Talebizadeh [10] reported that various small RNA molecules, including microRNAs (miRNAs), can regulate gene expression.

RNA interference (RNAi) is a gene-silencing technique that can be used to assess gene function, alter plant metabolic activities, and develop stress-tolerant and disease-resistant crops. For example, RNAi-mediated gene silencing has been demonstrated to serve as a defense mechanism against abiotic stresses [11–13]. Several studies have highlighted the importance of small RNA (sRNA) biogenesis, particularly miRNAs, in regulating plant responses to drought and other abiotic stresses [14–19]. Numerous plant regulatory networks are formed by miRNAs and their targets to regulate the overall plant response to stressors like drought [20]. Previously, RNAi-related enzymes were predominantly identified as junk DNA segments due to their small sizes [21].

RNA silencing is a conserved pathway involved in the regulation of growth, development, and abiotic stress responses. RNAi-related genes are key regulatory RNAs that control various plant biological processes, with miRNAs and siRNAs being the most important regulators of plant abiotic stress responses. They represent novel technologies for crop improvement [22].

Three main effector proteins are involved in RNAi: Argonautes (AGOs), Dicer-like proteins (DCLs), and RNA-dependent RNA polymerases (RDRs). These proteins play crucial roles in the RNA silencing machinery, forming RNA-induced silencing complexes with sRNAs, such as siRNAs and miRNAs, thereby triggering sequence-specific destruction or suppression of mRNA translation [23–26]. The biogenesis and regulation of sRNAs are controlled by AGO, DCL, and RDR proteins [27–31]. AGO, DCL, and RDR proteins contribute to gene-silencing processes during stress response and plant development [32]. miRNA expression levels change when exposed to drought, salinity, temperature variations, and oxidative environments, leading to the modulation of target gene expression associated with the abiotic stress response. Despite promising progress in understanding the function of sRNA biogenesis genes in plant growth and development, information related to their role in regulating drought stress response is limited, especially in fruit trees [13]. *Cis*-regulatory elements are regions of non-coding DNA that regulate genes transcription, and include silencers, promoters, and enhancers [33]. Moreover, *cis*-regulatory elements are thought to vary based on genetic and evolutionary properties and genes characterization [34]. Beneficial *cis*-regulatory variants are more likely to have a key role in the course of evolution. [33].

In this study, RNAi-related genes in the peach plant were identified, and their expression in response to drought stress was analyzed. The results shed light on the application of sRNA biogenesis to improve the drought tolerance of peach tree plants through molecular breeding.

2. Results

2.1. Identification and Characterization of RNAi-Related Genes in Rosaceae

The identified *PpAGO*, *PpDCL*, and *PpRDR* genes were named according to their phylogenetic relationships with the *Arabidopsis thaliana* sRNA biogenesis genes (Figure 1). A total of 11 PpAGOs were detected in the peach genome based on the structural integrity of

their conserved domains. In addition, phylogenetic analysis was performed to evaluate the relationships between peach and Arabidopsis AGO deduced proteins (Figure 1A). All the peach AGO proteins clearly form three clades: Clade I (AGO1/5/10), Clade II (AGO2/3/7), and Clade III (AGO4/6/8/9). Notably, despite having no orthologous members in the peach genome, three Arabidopsis proteins, including AGOs 8, 9, and 3, were clustered with other peach AGOs. They also shared similar physicochemical properties, such as amino acid length, with other peach AGOs in the same clade. Furthermore, the isoelectric point (*p*I), molecular weight (MW), and sequence length were analyzed for each identified gene (Table 1). The phylogenetic analysis was performed for peach DCLs (Figure 1B). PpDCLs were divided into four clades (I, II, III, and IV), and each DCL was clustered and named according to the clade.

Table 1. Genomic features and chemical properties of the predicted AGO, DCL and RDR proteins in peach.

Gene Name	Assigned ID	Chr. Location	Genomic (bp)	CDS (bp)	Protein (aa)	Mw (kDa)	*p*I	Seq. Source	Common Sub-Cell. Location
PpAGO1b	Prupe.5G241600	Chr5	7872	3210	1069	118.5	9.6	NCBI	Nucl.
PpAGO1a	Prupe.5G241500	Chr5	8521	3309	1102	121.6	9.7	NCBI	Cyto.
PpAGO2b	Prupe.4G108100	Chr4	4728	3192	1063	110.8	8.7	NCBI	Nucl.
PpAGO2a	Prupe.4G108000	Chr4	3499	2907	969	108.1	8.5	Phytozome	Nucl.
PpAGO4c	Prupe.6G154800	Chr6	8919	2820	939	104.2	8.6	NCBI	Nucl.
PpAGO4a	Prupe.2G056700	Chr2	8931	2736	911	101.7	9.5	NCBI	Nucl.
PpAGO4b	Prupe.2G056600	Chr2	8406	2619	873	97.8	9.7	Phytozome	Nucl.
PpAGO5 X1 *	Prupe.6G115400	Chr6	7057	3012	1003	111.9	9.8	NCBI	Mito.
PpAGO5 X2				2718	905			NCBI	Nucl.
PpAGO5 X3				2508	835			NCBI	Nucl.
PpAGO6	Prupe.3G209300	Chr3	7864	2697	898	100.3	8.7	NCBI	Nucl.
PpAGO7 X1	Prupe.1G279900	Chr1	4021	3042	1013	114.9	9.4	NCBI	Nucl.
PpAGO7 X2				3039	1012			NCBI	Nucl.
PpAGO10	Prupe.1G022900	Chr1	9159	2973	990	111.2	9.4	NCBI	Cyto.
PpDCL1	Prupe.2G200900	Chr2	10,239	5916	1971	220.3	5.8	NCBI	Nucl.
PpDCL2a	Prupe.7G048000	Chr7	4909	2346	781	88.9	6.3	NCBI	Nucl.
PpDCL2b	Prupe.7G047900	Chr7	5286	2349	782	88.8	6.1	NCBI	Nucl.
PpDCL2c X1	Prupe.7G047700	Chr7	23,773	2364	782	91.6	6.7	NCBI	Cyto.
PpDCL2c X2				2103	700			NCBI	Nucl.
PpDCL2	Prupe.6G363600	Chr6	10,785	4191	1396	159.5	6.4	NCBI	Nucl.
PpDCL3a X1	Prupe.1G401900	Chr1	10,655	5073	1690	183.7	6.1	NCBI	Nucl.
PpDCL3a X2				4935	1644			NCBI	Nucl.
PpDCL3a X3				4479	1492			NCBI	Nucl.
PpDCL3b	Prupe.8G202000	Chr8	8675	5025	1674	194.6	6.5	NCBI	Nucl.
PpDCL4 X1	Prupe.7G252800	Chr7	13,130	4926	1641	183.6	6.0	NCBI	Nucl.
PpDCL4 X2				4914	1637			NCBI	Nucl.
PpRDR1a X1	Prupe.4G078900	Chr4	4121	3435	1144	128.1	6.7	NCBI	Nucl.
PpRDR1a X2				3354	1117			NCBI	Nucl.
PpRDR1b	Prupe.4G078800	Chr4	4871	3084	1028	117.0	7.4	Phytozome	Nucl.
PpRDR1c	Prupe.1G334600	Chr1	5735	3372	1123	128.3	6.8	NCBI	Nucl.
PpRDR1d	Prupe.1G334500	Chr1	4636	3315	1104	124.4	6.6	NCBI	Cyto.
PpRDR1e	Prupe.1G332600	Chr1	5347	3774	1257	141.9	6.3	NCBI	Cyto.
PpRDR1f	Prupe.1G132100	Chr1	2487	2127	709	79.8	6.5	Phytozome	Chlo.
PpRDR2	Prupe.5G176700	Chr5	7653	3357	1118	127.4	6.4	NCBI	Chlo.
PpRDR4	Prupe.7G221200	Chr7	9707	3240	1079	122.0	7.1	NCBI	Nucl.
PpRDR6	Prupe.1G480300	Chr1	6593	3591	1196	136.4	6.8	NCBI	Nucl.

* X represent different isoforms. Nucl.: nucleus; Cyto.: cytoplasm; Chlo.: chloroplast; Mito.: mitochondria.

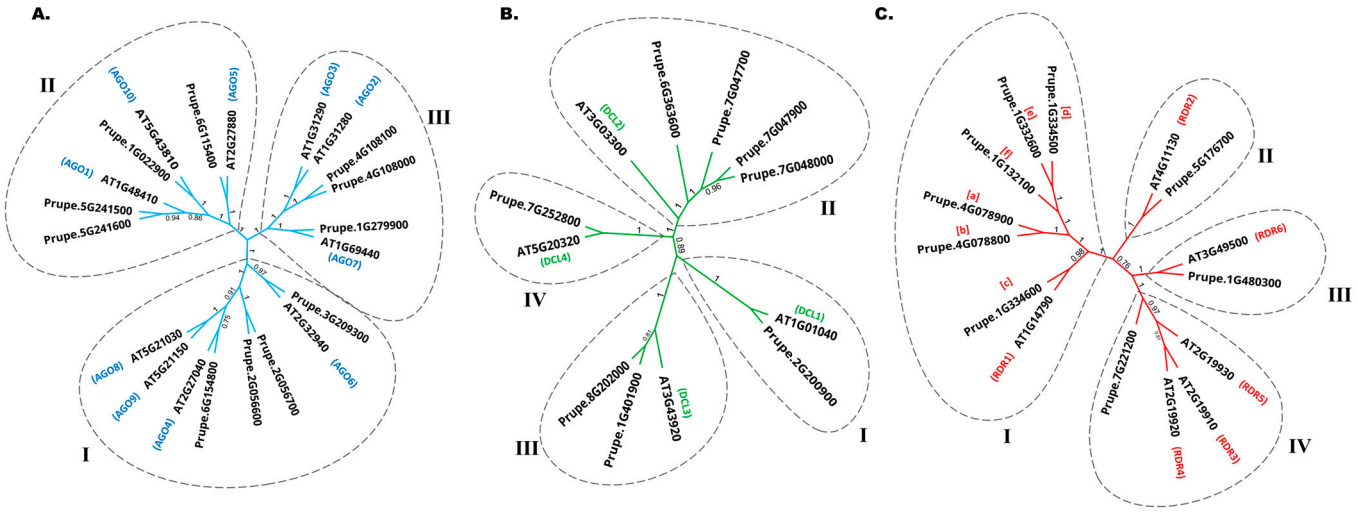

Figure 1. Phylogenetic analysis of peach AGOs, DCLs, and RDRs. (**A**) Phylogenetic tree for AGO deduced proteins from *P. persica* and *A. thaliana*. (**B**) Phylogenetic tree for DCL deduced proteins from *P. persica* and *A. thaliana*. (**C**) Phylogenetic tree for RDR deduced proteins from *P. persica*. and *A. thaliana*. All the phylogenetic trees were constructed using the neighbor-joining method, and the numbers at the nodes indicate the percentages of bootstrap values from 1000 replications. The clades of each tree were divided ascendingly by names using I, II, III, etc.

Based on the phylogenetic relationship between the peach and *A. thaliana* proteins, RDR proteins were divided into four clades (I, II, III, and IV) (Figure 1C). Clade I (RDR1) had the largest members of *PpRDRs: PpRDR1a*, *b*, *c*, *d*, *e*, and *f.* Each of Clade II (RDR2) and Clade III (RDR6) had only one *RDR* gene member. In Clade IV, *AtRDR3* and *AtRDR4* were grouped with *AtRDR5*, which blasted into one *PpRDR*5 (Prupe.7G221200).

To perform genome-wide identification of the AGO, DCL, and RDR gene families in the Genome Database for Rosaceae (GDR), all Hidden Markov Model (HMM) profiles of the conserved domains were gathered, and the identities of AGO, DCL, and RDR conserved domains were examined. A total of 97 *AGOs*, including 11 genes from peach, were identified in the genomes of the eight tested Rosaceae species (Table S1). Specifically, 10, 18, 10, 16, 14, 10, and 8 members were observed in strawberry (*Fragaria vesca*), China rose (*Rosa chinensis*), black raspberry (*Rubus occidentalis*), apple (*Malus* × *domestica*), pear (*Pyrus communis*), almond (*Prunus dulcis*), and Armenian plum (*Prunus armeniaca*), respectively, as shown in Figure 2A. To determine the evolutionary relationship among the orthologues of Rosaceae AGO proteins, a comprehensive neighbor-joining (NJ) phylogenetic tree was constructed. Notably, Clade III was the largest in the Rosaceae family with 38 members, while Clade II was the smallest with 25 members. The AGO4 members were split into two subclades, AGO4a and AGO4b, suggesting their expansion among the tested Rosaceae species. Additionally, the AGO8/9 and AGO3 subclades appeared to have been lost during the evolutionary process in the tested Rosaceae species.

In our previous study, a total of eight *PpDCL* genes were identified in the peach genome [35] (Table S2). For RDRs, the total of nine PpRDR members were equally grouped into four major clusters (Figure 2B). Furthermore, a total of 112 RDR transcripts were identified from the eight selected Rosaceae genomes (Table S3). Excluding the nine PpRDR copies, a total of 77 nonredundant RDRs were retrieved for further analysis, including 4, 13, 12, 9, 6, 10, and 14 copies from *F. vesca*, *R. chinensis*, *P. armeniaca*, *P. dulcis*, *R. occidentalis*, *P. communis*, and *M. x domestica*, respectively. All the obtained Rosaceae *RDR* genes were displayed in four clades, and each clade was outgrouped with *AtRDR*. Notably, the *PpAGO5* genes were clustered with *AtAGO5*, which is included with other *AtRDR3* and *AtRDR4* subfamilies, according to higher sequence similarity with *AtAGO5* (Figure 2B).

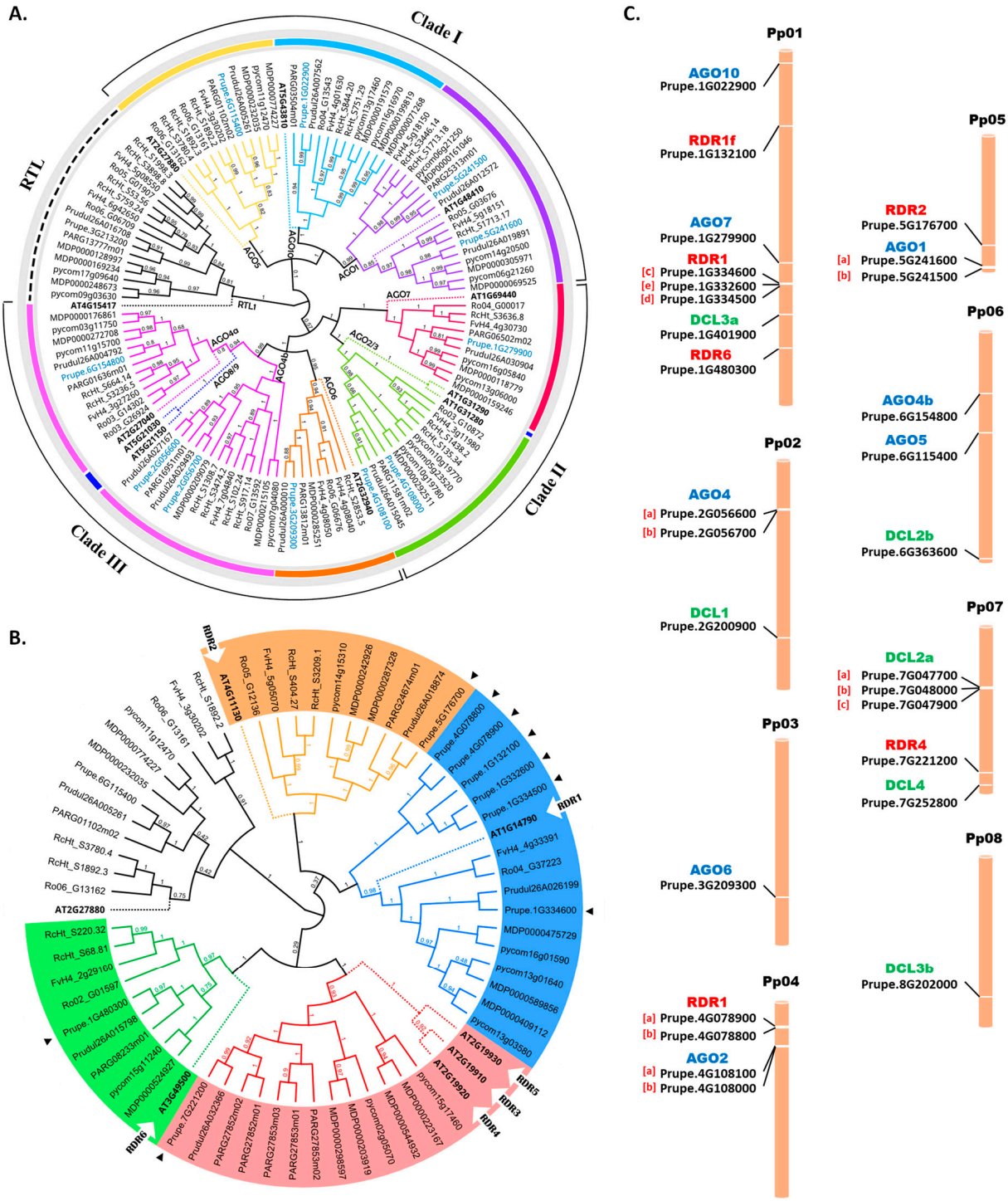

Figure 2. Phylogenetic analysis and gene chromosomal locations. (**A**) AGO protein family in Rosaceae. The AGO1/5/10, AGO2/3/7, AGO4/6/8/9 clades were named according to the 10 Arabidopsis AGOs. Blue fonts refer to the identified *AGO* genes. (**B**) RDR protein family in Rosaceae. The unrooted NJ tree was constructed in Geneious Prime 2023.1.1. with 1000 bootstrap replicates. RTL1 is rooted as an outgroup (No color), while the colored clades indicate the identified RDR gene members. (**C**) Chromosomal location of PpAGOs, PpDCLs, and PpRDRs. Tandemly duplicates are shown in square parenthesis.

2.2. Chromosomal Localization, and Evolutionary Analysis in P. persica

The localization of predicted *AGO*, *DCL*, and *RDR* genes across the eight chromosomes in the peach genome was performed through a BLAST search to determine the physical location of each gene. As a result, the 11 *AGO* genes were unevenly distributed across the eight chromosomes (Figure 2C). Notably, Chr2, Chr4, and Chr5 contained three duplicate paralogous pairs, PpAGO4b/PpAGO4a, PpAGO2b/PpAGO2a, and PpAGO1b/PpAGO1a, respectively; while Chr1 and Chr6 contained two *AGO* genes each, including PpAGO10, PpAGO7, and PpAGO5/PpAGO4c, respectively. The Arabidopsis *AGO4* gene mapped to three duplicated members in the peach genome, including PpAGO4a, PpAGO4b, and PpAGO4c, with the latter two genes being tandemly duplicated. The adjacency of these genes indicates that they originated through tandem duplication events, suggesting that tandem duplication is a key evolutionary process driving the expansion of this gene family in the peach genome.

The distribution of *DCL* genes in the peach genome showed that the eight predicted *DCL* genes could be mapped on five out of the eight chromosomes (Figure 2C).

The nine identified *PpRDR* genes are located on four chromosomes (Chr1, Chr4, Chr5, and Chr7). Chr1 contained the majority of *PpRDR* genes (five genes), although it is the longest chromosome. The results showed that *PpRDR* genes, such as the paralogous pair of PpRDR1a (Prupe.4G078900) and PpRDR1b (Prupe.4G078800), were closely located on Chr4. The existence of homologous genes in the same location indicates that these genes originated by tandem duplication, giving rise to paralogous genes. Tandem duplication is frequently regarded as a primary factor driving various biological functions. Similarly, triple duplications of PpRDR1c, PpRDR1d, and PpRDR1e (Prupe.1G334600, Prupe.1G334500, and Prupe.1G332600, respectively) were located on Chr1. The results indicate that duplicated genes may have complex phylogenetic structures due to variations in their evolutionary alterations.

The duplication of PpRDRs is centralized on four chromosomes, making it interesting to study the characteristics of phylogenetic relationships in different species. Triple copies or multi-gene sets of putative orthologs may contain paralogs that have not been detected. Notably, some *PpRDR* genes, such as PpRDR3 and PpRDR5, are absent, as shown in the phylogenetic tree (Figure 2C) and NJ clusters (Figure 1C). This absence might be due to a high similarity between the reference genome sequences of *AtAGO* and *AtRDR* and their peach counterparts, leading to the absence of PpRDR3 and PpRDR5 in the BLAST results. The similarity between these genes includes molecular properties such as sequence length (992 and 977 amino acids) and molecular weight (112.8 and 110.9 kDa), respectively. *AtRDR3* and *AtRDR5* cluster as siblings with *AtRDR4* in the same clade. This high similarity may explain why PpRDR3 and PpRDR5 were not detected in the peach genome, possibly due to data processing deletions or resulting isoform copies of genes.

2.3. Gene Structure and Motif Analysis in P. persica

To further validate and gain insights into the potential activities of the identified peach sRNA biogenesis proteins, we analyzed their gene structure and conserved regions involved in RNA binding, enzyme catalysis, and other critical features. Previous studies have demonstrated that these predicted domains play crucial roles in protein activity in plants [36,37]. The functional domain analysis revealed that most peach AGO, DCL, and RDR proteins are highly conserved (Figure 3).

Peach AGO proteins are primarily characterized by three domains, PAZ, MID, and PIWI (Figure 3A), consistent with previous studies [38–40]. It has been reported that the PAZ and PIWI domains play critical roles in RNase activity in AGOs [12,41,42]. Both PAZ and PIWI domains were detected in all the putative PpAGO proteins, showing similarities with their Arabidopsis orthologs. The PAZ domain is essential for binding the 2-nt 3′ overhang of sRNAs, while the PIWI domain of certain AGOs has RNase activity [37,43]. The MID domain anchors the 5′ phosphate end of sRNAs onto Argonaute proteins [37,41,44–47]. The putative PpAGO6 (Prupe.3G209300) was highlighted for structural prediction and

generic domain structure analysis of AGOs. PpAGO6 has a protein length of 898 amino acids. The PAZ domain is located between residues D283 and S381 (99 amino acids in length), while the PIWI domain is located between F550 and K859 (310 amino acids in length). Both domains showed identical homology with RNase H, which binds to the 5′ end of the siRNA of the target RNA and cleaves it, demonstrating that sRNAs are complementary sequences [48,49].

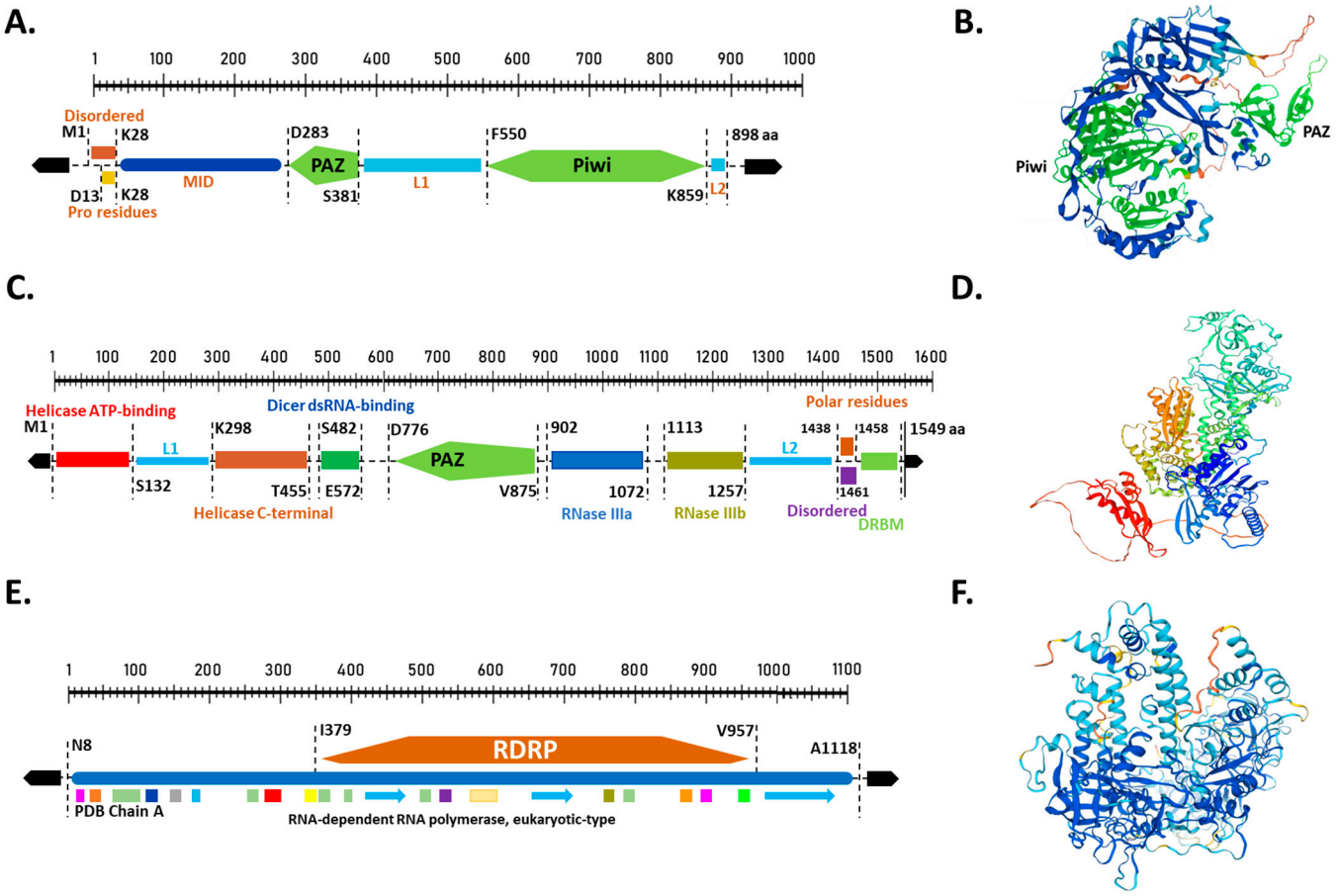

Figure 3. Illustrates the gene structure and crystal modeling of PpAGO6 (**A**,**B**), PpDCL4 (**C**,**D**), and PpRDR2 (**E**,**F**) proteins. (**A**) Schematic domain architecture of PpAGO6 proteins. (**B**) Representative crystal structure of full-length PpAGO6 protein. (**C**) Schematic domain architecture of PpDCL4 proteins. (**D**) Representative crystal structure of full-length PpDCL4 protein. (**E**) Schematic domain architecture of PpRDR2 proteins. (**F**) Representative crystal structure of full-length PpRDR2 protein. The displayed colors were similarly applied from the 3D forms into the protein structure.

The residues of AGO domains are involved in sRNA binding, sorting, and sRNA-targeted RNA pairing. sRNA sorting into different AGOs depends on features such as sRNA length and 5′ end nucleotide type [50–52]. sRNA 5′ terminal nucleotide of sRNA is recognized by the nucleotide specificity loop within the MID domain (Figure 3A). The MID domain is reported to be the main component of AGO with crucial functions in RNA silencing [51,53]. Additionally, other highly conserved residues or motifs with potential functional importance were detected within the 3′ end of sRNAs. These motifs are labeled as 'L' in Figure 3A.

Dicer-like (DCL) proteins are endonucleases with two RNase III domains [54–56]. DCL proteins split both strands near the terminal loop to generate the miRNA duplex, containing the miRNA paired with its passenger strand. Figure 3C presents PpDCL4 as an example model of peach Dicer-like proteins. PpDCL4 is composed of six functional parts: the PAZ domain (residues D776–V875), two helicase binding fragments, Dicer

dsRNA-binding residues, and two RNase III domains. The PAZ domain is connected to RNase IIIa on one side, while the helicase C-terminal contacts the PAZ domain from the opposite direction through Dicer dsRNA-binding residues. RNase-IIIb follows RNase IIIa in structure. The helicase binding fragments include helicase ATP-binding (M1–S132) and helicase C-terminal (K298–T455), while the Dicer dsRNA-binding domain is located between S482 and E572. RNase-IIIa and RNase-IIIb, located between positions 902–1072 and 1113–1257, respectively, are the main components of DCL domains and interact directly with substrate RNAs. The overall structure of DCL domains resembles a hacksaw [56].

The structure of PpRDR and the distribution of domains along the PpRDR sequence are depicted schematically in Figure 3E. *PpRDR2* has a canonical RNA-dependent RNA polymerase (RDRP) domain characteristic of known polymerase structures, with the PDB chain regions playing an important role in the observed structure. The RDRP domain occupies the largest part of the PpRDR2 protein sequence, spanning 579 amino acids in length (I379–V957).

The Protein Data Bank (PDB) format is shown as a standard for files containing atomic coordinates. Using the Swiss-Model for online analysis, we found that the tertiary amino acid sequences of 28 members were highly similar (Figure S1A–C). In this study, we modeled the amino acid sequences of 28 RNAi-related genes from the three gene families using 3D structural homology. One gene from each family was chosen for modeling, as shown in Figure S1.

The analysis focused on conserved motifs involved in RNA-binding, enzyme catalysis, and other critical features to characterize the identified *P. persica* silencing proteins. The predicted PpDCL, PpAGO, and PpRDR protein sequences were aligned with reference sequences of AtDCL, AtAGO, and AtRDR (Figure 4). Conserved functional motifs in PpAGOs were confirmed, such as Y950, K958, Q978, N991, K995, and I996, crucial for the MID domain's role in sRNA 5′-phosphate-binding [57], which were fully conserved across peach AGO proteins (Figure 4A). The PAZ domain residues (G1929, D1931, V1932, and H1934) were also universally present. Furthermore, the RDGVS (1118–1122 aa) motifs were conserved in all AGOs of peach and Arabidopsis. Examination of the PIWI domain revealed conserved residues like E1133, D1191, DE (1224 and 1125), and H1161, implicated in enzyme catalysis [40,43,58]. Further functional analysis is needed to elucidate the specific roles of these residues in PpAGO proteins. The glutamine–phenylalanine–valine (QF-V) motif critical for sRNA duplex recognition and sorting was conserved across all PpAGOs [39,40,59] (Figure 4A), suggesting their importance in sRNA 3′-end binding within PAZ and PIWI domains.

To assess the functional similarity of peach DCL proteins with Arabidopsis counterparts, we conducted multiple sequence alignments and motif composition analyses. Computational modeling of the catalytic core of AtDCL4 provided insights into the amino acids critical for dsRNA recognition, binding, and cleavage. The alignment revealed conserved RNase IIIa, RNase IIIb, and an RNA binding motif across PpDCL proteins (Figure 4B). Specifically, the RNase III catalytic sites of peach DCL proteins featured glutamate (E), aspartate (D), aspartate (D), and glutamate (E) (EDDE), analogous to their orthologs in AtDCLs. Key residues include E1513, D1517, D1642, and E1645 for RNase IIIa, and E1737, D1741, D1745, and E1838 for RNase IIIb, with the RNA-binding motif characterized by the H-S loop (Figure 4B). Additionally, sequence alignment of AtRDRs with putative PpRDR proteins identified the conserved D-DGD catalytic motif, a hallmark of the RDR conserved domain (Figure 4C).

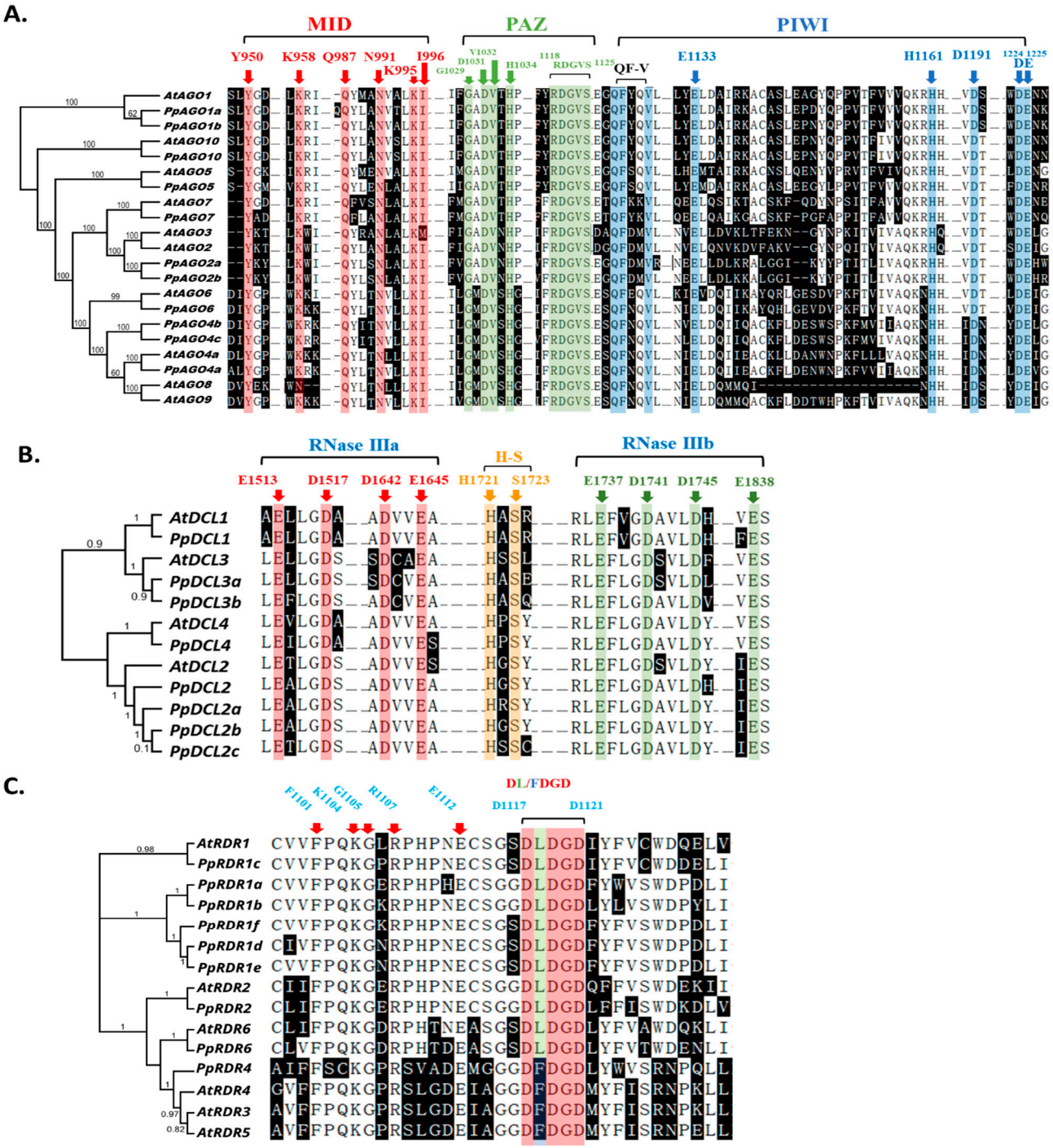

Figure 4. Multiple sequence alignment results of AGOs, DCLs, and RDRs showing conserved bases in the motifs. The phylogenetic clades are shown on the left. (**A**) Functionally conserved positions within MID, PAZ, and PIWI domains of *A. thaliana* and peach AGO proteins. Residues within the MID domain (indicated by red arrows) crucial for sRNA-target interaction (I996), 5′ terminal nucleotide selection (N991), and 5′-phosphate-binding (YKQK) residues. PIWI domain (blue arrows) highlights the catalytic tetrad (EHDDE) and QF-V motif. Residue numbers correspond to AtAGO1 amino acid positions. (**B**) Conservation of functionally critical amino acids between *A. thaliana* and peach DCL proteins. Conserved residues involved in enzyme catalysis within RNase IIIa (E1513, D1517, D1642, E1645; red arrows), RNase IIIb (E1737, D1741, D1745, E1838; green shading and arrows), and RNA-binding motifs (H-S motif; yellow shading and arrows). (**C**) Presence of functionally critical amino acid residues in peach RDR proteins. The catalytic domain (D[L/F]DGD) within RdRP is highlighted.

2.4. Orthologous Similarity and Collinearity Analysis for Non-Coding RNA Genes

Our analysis indicated that most gene pairs have a less mutation characteristic of evolutionary constraint, thus nonsynonymous site (Ka), in a given period, to the number of synonymous substitutions per synonymous site (Ks) Ka/Ks ratio < 1, signifying a strong purifying selection and underscoring their essential roles in plant fitness under stressful conditions. Notably, significant sequence similarities were identified between peach and Arabidopsis AGO orthologs (Figure 5A). AtDCL1 exhibited the highest similarity score among peach DCLs with its ortholog, scoring ≥ 0.75, followed by AtDCL2 and AtDCL4 with scores ≤ 0.50, while AtDCL3 showed lower similarity with its orthologous genes.

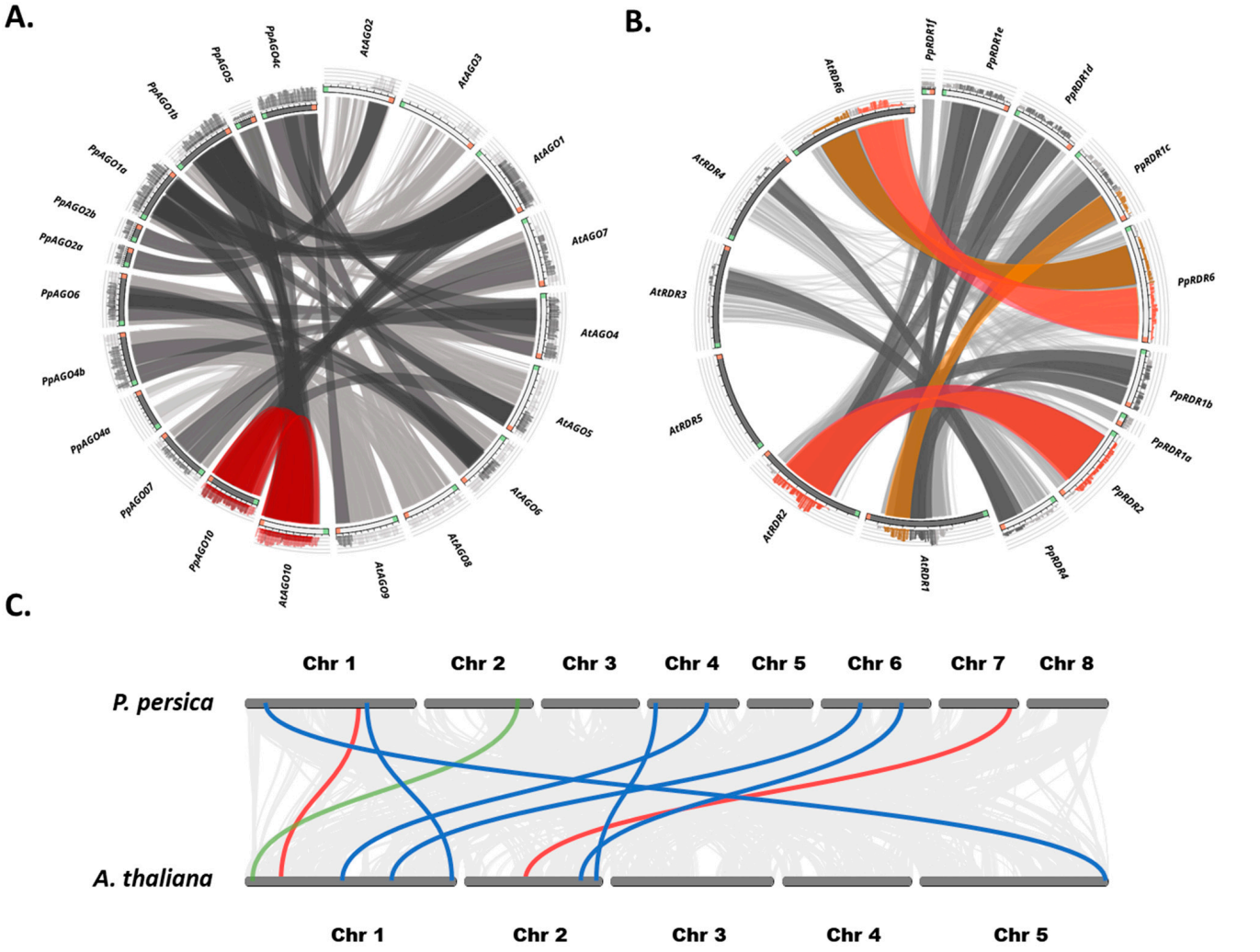

Figure 5. Orthologous similarity and collinearity analysis of sRNA biogenesis genes in peach and Arabidopsis. (**A**) Circos plot depicting the similarity among identified AGO orthologs. (**B**) Circos plot illustrating the similarity among identified RDR orthologs. The highlighted arcs in the center of the Circos plots connect orthologous sRNA biogenesis genes. Interprotein arcs represent significant similarities with *p*-values < 0.05, distinguished by red (>99% identity), brown (95–99%), and gray lines (90–95%) indicating tandem, WGD/segmental duplicates, and other similarities, respectively. (**C**) Genome-wide collinearity of AGOs (blue), DCLs (green), and RDRs (red) between Arabidopsis and peach chromosomes. Lines connect collinear blocks of gene pairs.

RDR genes were mapped using Blastp protein sequence comparisons [59], revealing distinct similarity patterns between PpRDRs and their AtRDR orthologs (Figure 5B). *PpRDR1* genes comprised six copies (PpRDR1a to PpRDR1f), each showing high similarity with specific AtRDR counterparts, whereas other AtRDR genes exhibited less similarity with their duplicates. PpRDR2, PpRDR4, and PpRDR6 each showed varying degrees of similarity with different AtRDRs, with PpRDR6 (Prupe.1G480300) demonstrating the highest similarity score among all copies, followed by PpRDR2 (Prupe.5G176700).

Additionally, chromosomal collinearity analyses of AGOs, DCLs, and RDRs (Figure 5C) revealed extensive conservation between peach and Arabidopsis. Five AGO genomic collinear pairs exhibited shared gene order: PpAGO7-AtAGO7, PpAGO10-AtAGO10, PpAGO6-AtAGO6, PpAGO2a-AtAGO2, PpAGO1a-AtAGO1, and PpAGO5-AtAGO5. DCLs showed lower collinearity with only one pair (PpDCL1-AtDCL1) maintaining collinearity. For RDRs, two collinear regions were identified: PpRDR1d-AtRDR1 and PpRDR4-AtRDR4. These findings underscore a conserved genomic structure between these species across the three non-coding small RNA gene families.

Predicted *cis*-acting elements in the promoter regions were identified for all candidate *AGOs*, *DCLs*, and *RDRs* genes, classified into three functional groups: phytohormone-responsive, specific expression and stress-related, and light responsive–related. A total of 41, 40, and 42 promoter *cis*-acting elements were identified in PpAGOs, PpDCLs, and PpRDRs, respectively (Figure S2). Predominantly, these elements were associated with specific expression and stress response, highlighting their crucial roles in both biotic and abiotic stress responses (Figure S2). Notably, the analysis revealed a prevalence of CAAT-boxes and TATA-boxes across all AGOs, DCLs, and RDRs, underscoring their importance in transcriptional regulation. Additionally, TC-rich repeats, LTRs, and MBS promoters known to regulate responses to biotic and abiotic stresses [60] were prominently represented, indicating their direct involvement in the regulation of sRNA biogenesis genes, particularly under drought conditions (Figure S2) [61,62].

In *AGO* genes, promoter regions such as TAG-box and TATC-box, HD-Zip 1, A-box, CCAAT-box, and LAMP-element were specifically detected in *PpAGO6*, *PpAGO7*, *PpAGO1a*, *PpAGO2a*, and *PpAGO10*, respectively (Figure S2A). The analysis revealed consistent patterns of promoter *cis*-elements across homologous genes. For example, *PpAGO1a* and *PpAGO1b* exhibited 11 shared representations and 18 absences out of a total of 41 promoter regions. In *DCL* genes, MSA-like and MRE elements were identified exclusively in *PpDCL3a*, whereas A-box, HD-Zip3, AAAC-motif, and AT1-motif were present only in *PpDCL3b*. Additionally, Box II and chs-CMA2a were found in *PpDCL1* and *PpDCL4*, respectively (Figure S2B). Similar expression patterns were observed among paralogous genes, with *PpDCL2a*, *PpDCL2b*, and *PpDCL2c* sharing six representations and 18 absences. Moreover, PpDCL3a and PpDCL3b showed 10 shared representations and 6 absences out of a total of 40 promoter regions. In *RDR* genes, the Sp1 promoter region was identified uniquely in the *PpRDR1b* gene, while the ATC-motif and Circadian elements were present in *PpRDR1c* and *PpRDR1d*, respectively. Furthermore, Box III and ACE promoter regions were specific to the *PpRDR1f* gene sequence. Conversely, the GARE-motif and LAMP-element were exclusively detected in *PpRDR2*. Additionally, the TGA-box, AACA-motif, and A-box promoter regions were found only in *PpRDR4*, while chs-Unit1 m1 was identified in *PpRDR6* (Figure S2C). Similar patterns were observed among the six paralogous genes of *PpRDR1*, with five shared representations and 11 absences identified in the promoter *cis*-elements.

2.5. Expression Patterns of AGO, DCL, and RDR Genes in Peach Under Drought Stress

To predict the functions of *AGO* genes in peach, we analyzed their FPKM expression across different tissues including leaf, fruit, phloem, root, flower, and seed using available transcriptome data (v2.0.a1) (Figure 6A). Our findings revealed widespread expression of all peach AGOs across multiple tissues. Notably, *PpAGO2a* exhibited highest expression in roots followed by *PpAGO2b*, while *PpAGO2b* and *PpAGO4c* were prominently expressed in leaves, indicating potential roles in drought stress response. Particularly, *PpAGO2b* showed

predominant expression in leaves, roots, and phloem tissues. These insights contribute to understanding the evolutionary dynamics of *AGO* genes in Rosaceae and their roles in peach's response to drought stress.

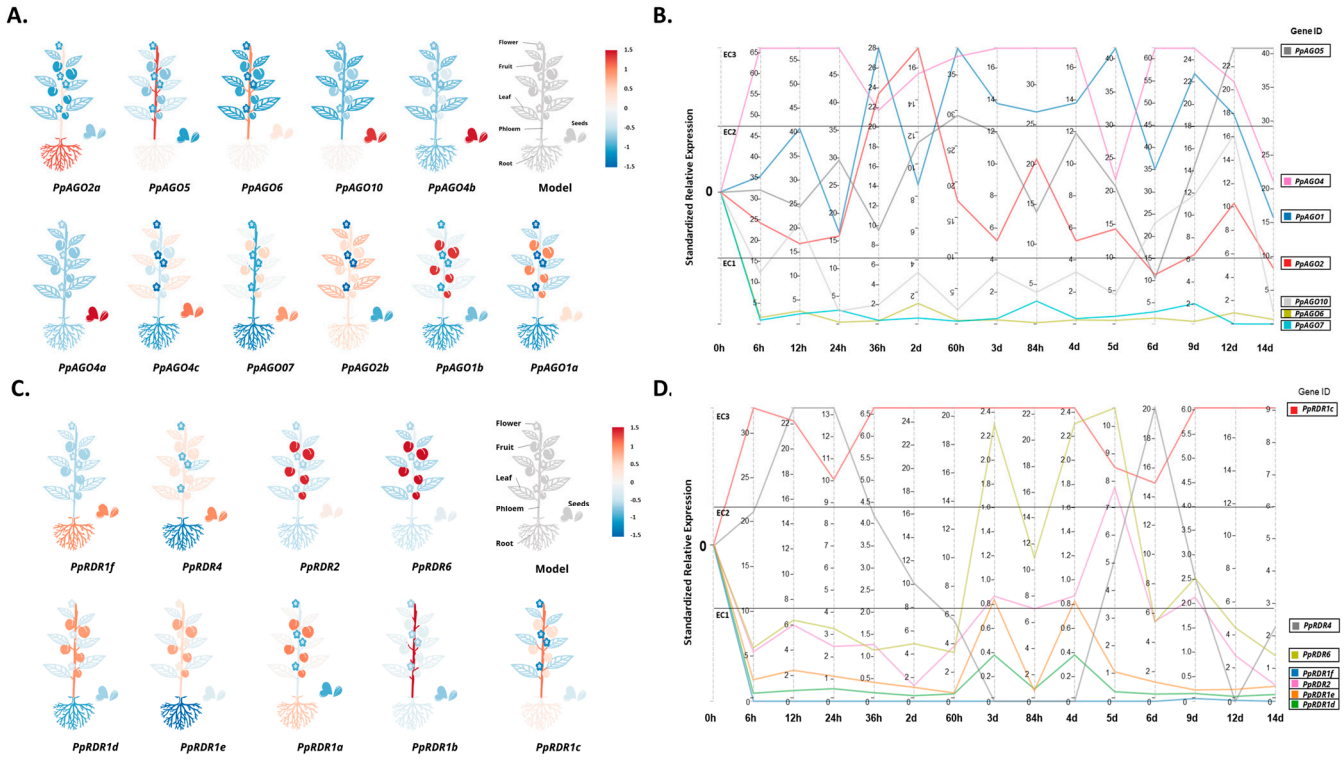

Figure 6. Tissues and temporal FPKM expression trends. FPKM analysis of *PpAGO* (**A**,**B**), *PpDCL* (Figure S3), and *PpRDR* (**C**,**D**) genes in various peach tissues under drought stress. Left panels show high expression levels of *PpAGO*, *PpDCL*, and *PpRDR* genes observed in peach seeds, fruits, roots, leaves, phloem, and flowers. Right panels depict temporal expression trends of *AGO*, *DCL*, and *RDR* genes in the fruit flesh of *P. persica* exposed to drought stress over a 14-day period, with 0 h as the control. Expression profiles are categorized into three clusters (EC1, EC2, and EC3) based on standardized relative expression levels. RNA data were used to assess the expression of *PpAGO*, *PpDCL*, and *PpRDR* genes.

Time-course expression analysis of *AGO* genes under drought stress further demonstrated differential expression patterns across peach tissues (Figure 6B). *PpAGO4c* exhibited peak expression on the first day of prolonged drought treatment but downregulated at subsequent time points (36 h, 5 days, and 14 days). Conversely, *PpAGO1a*, *PpAGO2b*, *PpAGO5*, and *PpAGO10* showed varying upregulation profiles under prolonged drought conditions. Conversely, *PpAGO1b*, *PpAGO2a*, *PpAGO4b*, *PpAGO4a*, *PpAGO6*, and *PpAGO7* displayed low relative expression in expression cluster 1 (EC1), suggesting potential co-expression in inducing drought resistance mechanisms under prolonged stress. Notably, phylogenetic analysis clustered *PpAGO4c*, *PpAGO4b*, and *PpAGO4a* closely together, suggesting functional redundancy or neo-functionalization in evolution (Figure 6B).

Environmental stresses profoundly influence plant gene regulation and adaptation. Stress-related genes are induced under adverse conditions to bolster plant resilience. Expression patterns of *PpDCL* genes under drought stress have been previously investigated [33] and are further detailed in supplementary results (Figure S3).

RDR genes, crucial in small RNA biogenesis, play pivotal roles in plant growth and development [63–66]. Expression patterns of *PpRDR* genes across six tissues (root, fruit, seed, flower, phloem, and leaf) were analyzed to infer their functional roles (Figure 6C).

All *PpRDR* genes were found to be expressed in these tissues, each exhibiting distinct expression patterns indicative of their roles in stress responses and development.

To delineate *PpRDR* gene functions under drought stress, their expression patterns were analyzed across different time points (Figure 6D). All *PpRDRs* displayed differential expression across expression clusters (EC) in response to short-term and prolonged drought conditions. For instance, *PpRDR1c* exhibited stable and elevated expression initially but decreased later, while *PpRDR4* showed dramatic fluctuations in expression levels across various time points. *PpRDR2* and *PpRDR6* showed parallel expression patterns, with *PpRDR6* displaying higher expression in EC2 and EC3. Conversely, *PpRDR1b* exhibited the lowest expression among *PpRDR1* copies in EC1, suggesting a potential role as a chronic co-expression gene in drought resilience. The expression of *PpRDR1* copies (d, e, and f) was significantly upregulated under prolonged drought stress from 3 to 12 days, indicating functional redundancy or neo-functionalization within this clade. These findings provide valuable insights into the molecular evolution and adaptive responses of *PpRDR* genes in Rosaceae, particularly in the context of drought stress in peach cultivation regions [6].

PpRDR4 exhibited a distinctive expression pattern characterized by a sharp increase within the first 12 h, followed by stable expression for the subsequent 12 h, and a dramatic decline within 2 days of treatment. It then stabilized for a day until a notable increase was observed on the sixth day, followed by another decline on day 12, and a subsequent increase on day 14. *PpRDR2* and *PpRDR6* displayed similar expression patterns, although *PpRDR6* showed enhanced expression in EC2 and EC3. Conversely, *PpRDR1b* exhibited the lowest expression during the initial phase of drought treatment in EC1, while *PpRDR1f* and *PpRDR1a* showed no significant expression patterns, implying their potential roles as constitutive co-expressed genes in drought resistance (Figure 6D). Expression of *PpRDR1* copies (d, e, and f) was significantly upregulated from days 3 to 12 of drought stress, whereas other genes from the same clade as *PpRDR1* remained unchanged, suggesting functional redundancy or neo-functionalization from a common ancestor during evolution. These findings offer insights into the molecular evolution of *PpRDR* genes within Rosaceae and their likely contributions to drought response in peach, a crop commonly cultivated in irrigated semi-arid and arid regions [6].

2.6. Quantitative Real-Time PCR (qRT-PCR) Validation of AGO, DCL, and RDR Genes

To gain insights into the roles of *AGOs*, *DCLs*, and *RDRs* in drought stress response, we assessed the expression of *PpAGO*, *PpDCL*, and *PpRDR* genes in two *P. persica* cultivars, 'BJ2-7' and 'SN' peach, known for their differing drought tolerance levels. Five candidate genes from each gene family were selected for qPCR analysis. Our findings revealed that under drought stress conditions, *PpAGO2a* and *PpAGO2b* genes were significantly induced in the leaves and roots of both cultivars. Notably, their expression was markedly higher in the leaves of 'BJ2-7' compared to 'SN'. In contrast, drought stress inhibited the expression of *PpAGO4c* and *PpAGO10* in the leaves of both cultivars, with *PpAGO4c* showing higher expression in 'BJ2-7' and *PpAGO10* in 'SN'. Additionally, *PpAGO5* was induced only in the leaves and roots of 'BJ2-7' but inhibited in 'SN', suggesting a potential role in drought tolerance specific to 'BJ2-7' (Figure 7A).

Among the *DCL* genes, 14 days of drought stress induced the expression of *PpDCL1*, *PpDCL2a*, *PpDCL3a*, and *PpDCL4* in the leaves of both cultivars (Figure 7B). Conversely, *PpDCL2b* was downregulated in response to drought stress in both cultivars. Interestingly, the induction of *PpDCL2a*, *PpDCL2b*, *PpDCL3a*, and *PpDCL4* was significantly higher in the leaves of 'BJ2-7' compared to 'SN'. Moreover, *PpDCL2b* and *PpDCL4* were induced only in the roots of 'BJ2-7' but inhibited in 'SN', while *PpDCL1* was inhibited in the roots of both cultivars, albeit with higher expression in 'BJ2-7' (Figure 7B).

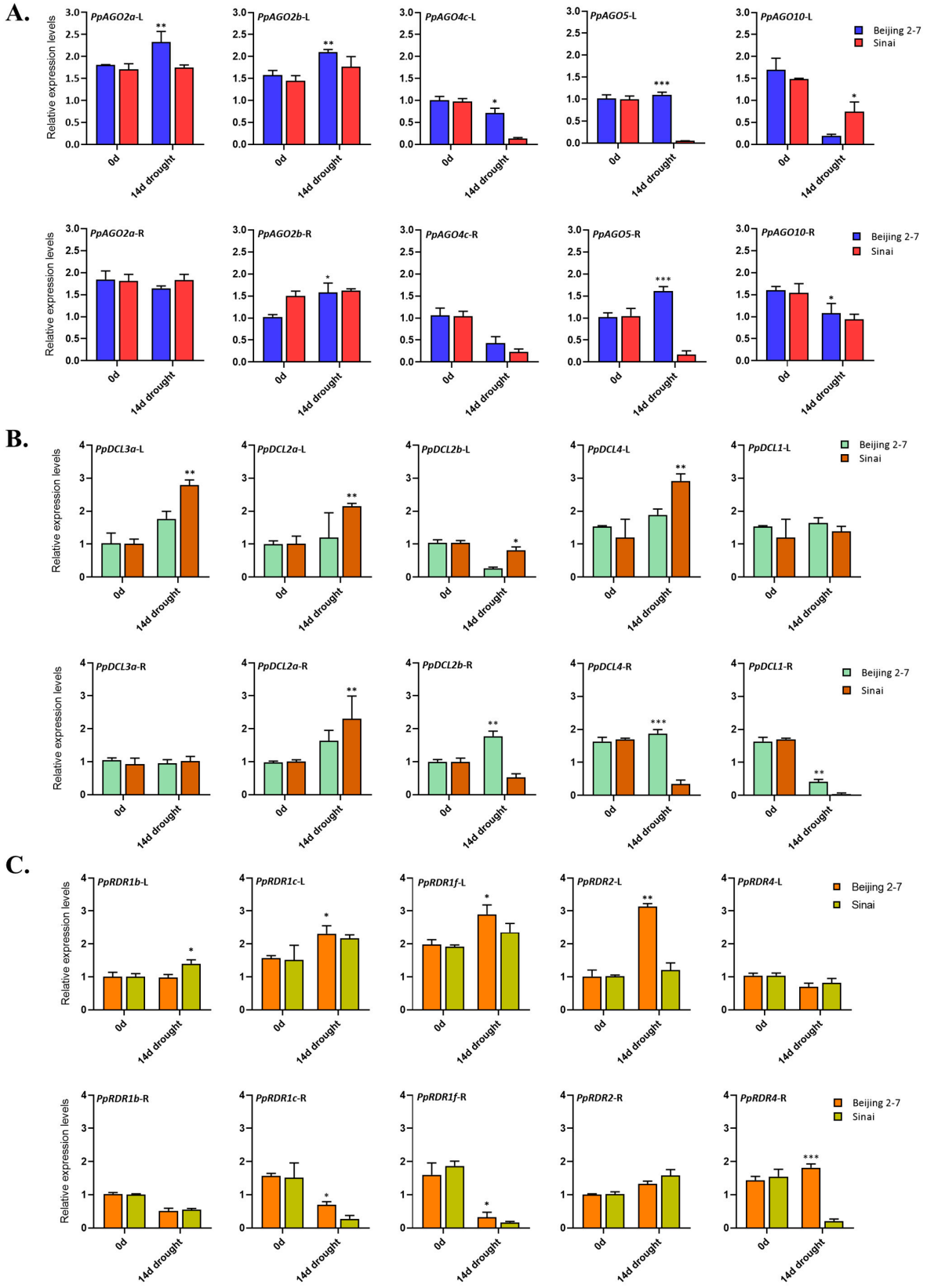

Figure 7. Relative expression of candidate genes in the leaves (-L) and roots (-R) of 'BJ2-7' and 'SN' peach cultivars under drought stress. (**A**) Expression of *PpAGO* genes. (**B**) Expression of *PpDCL* genes. (**C**) Expression of *PpRDR* genes. Plants were exposed to drought stress for 14 days, with control plants receiving regular watering. Data are presented as means ± standard errors ($n = 3$). Asterisks indicate significant differences at * $p < 0.05$, ** $p < 0.01$, and *** $p < 0.001$ based on Student's *t*-test.

In the case of *RDR* genes, drought stress induced the expression of *PpRDR1b*, *PpRDR1c*, and *PpRDR1f* in the leaves but inhibited them in the roots of both cultivars (Figure 7C). Interestingly, the expression levels of *PpRDR1b* and *PpRDR1f* in the leaves, and *PpRDR1c* in the roots, were significantly higher in 'BJ2-7' compared to 'SN'. Although *PpRDR2* expression was induced by drought stress in both cultivars, it was inhibited in the leaves of 'BJ2-7' while unaffected in 'SN'. Furthermore, drought stress inhibited the expression of *PpRDR4* in the leaves of both cultivars, whereas its expression was induced only in the roots of 'BJ2-7' but inhibited in 'SN' (Figure 7C). These results highlight the differential responses of *AGO*, *DCL*, and *RDR* genes to drought stress in peach cultivars with varying tolerance levels, providing valuable insights into their roles in drought adaptation mechanisms.

2.7. Analysis of Plant Biomass, Electrolyte Leakage (EL), Proline Content, and Total Soluble Sugar Content in Peach Cultivars Under Drought Stress

The physiological and biochemical analyses revealed that the Chinese peach cultivar 'BJ2-7' exhibits greater drought resistance compared to the Egyptian peach cultivar 'SN'. As illustrated in Figure 8, 'SN' exhibited a substantial biomass decrease (48.8%) under drought stress, whereas 'BJ2-7' showed a much lower reduction (10.7%). Additionally, the results of electrolyte leakage (EL) indicated weakened cell wall integrity under severe drought conditions, with a significant increase observed after 14 days. EL percentage was notably higher in the 'SN' cultivar compared to 'BJ2-7', suggesting greater tissue damage in 'SN' under drought conditions. Furthermore, Figure 8C shows that 'BJ2-7' recorded the highest proline content after 14 days of drought stress (3.85 µg/g), while 'SN' exhibited the lowest proline levels during the same period.

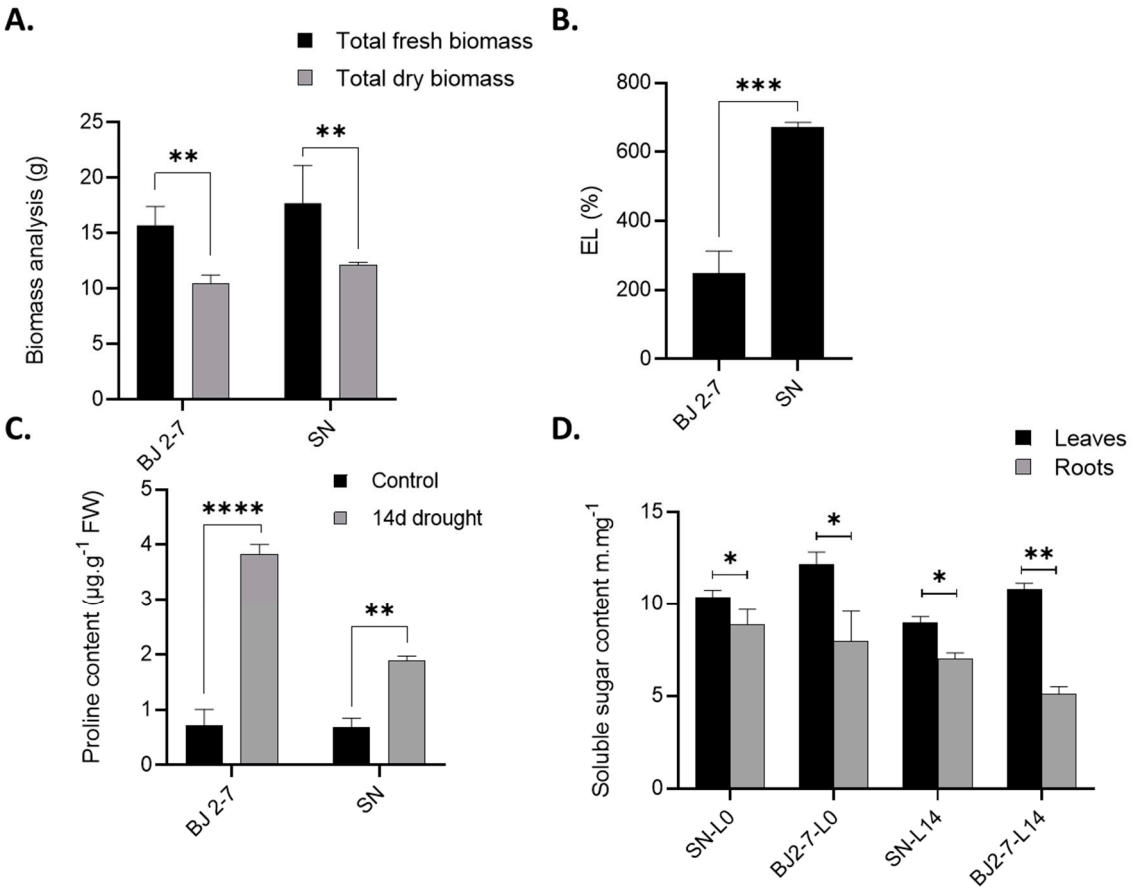

Figure 8. Physiological and biochemical traits analysis. (**A**) Biomass analysis. (**B**) Electrolyte leakage percentage. (**C**) Proline content. (**D**) Soluble sugar contents. Data are presented as means ± standard errors (n = 3). * $p < 0.05$, ** $p < 0.01$, *** $p < 0.001$, and **** $p < 0.0001$ based on Student's t-test.

To investigate how drought affects sugar metabolism and distribution between leaves and roots in peach cultivars 'SN' and 'BJ2-7', we analyzed the total soluble sugar content. Interestingly, under 14 days of drought stress, 'BJ2-7' exhibited higher accumulation of total soluble sugars in its leaves compared to 'SN'. Conversely, in the roots, 'SN' showed a higher accumulation of total soluble sugars compared to 'BJ2-7' (Figure 8D). Under control conditions, 'BJ2-7' accumulated significantly more total soluble sugars in its leaves compared to 'SN', whereas in roots, 'SN' accumulated more total soluble sugars compared to 'BJ2-7'.

3. Discussion

Peach (*P. persica* L.) is a globally significant crop grown in temperate climates, yet its survival and productivity are vulnerable to environmental stresses [5,6]. Small RNA (sRNA) biogenesis genes play pivotal roles in regulating chromatin structure at the transcriptional level during plant growth and development [67,68]. Consequently, RNA silencing represents a conserved pathway essential for modulating growth, development, and responses to abiotic stresses [20,69]. Central to RNA silencing are key components including AGOs, DCLs, and RDRs. Despite the economic importance of peach, comprehensive studies elucidating its RNA silencing pathways and regulation have been lacking [35]. In this study, systematic genome-wide screening identified 11 AGOs, 8 DCLs, and 9 RDRs as candidate genes in peach. While these gene families have been extensively studied in other plants, their characterization in peach has been limited.

Recent genome-wide analyses and phylogenetic studies have identified a range of small RNA (sRNA) biogenesis genes across various plant species. For instance, diploid strawberry revealed 13 AGOs, 6 DCLs, and 9 RDRs candidates [70], while tea exhibited 18 AGOs, 5 DCLs, and 9 RDRs candidates [71]. Similarly, banana showed 13 AGOs, 3 DCLs, and 5 *RDRs* candidate genes, and the modern sugarcane cultivar genome [72], contained 21 AGOs, 4 DCLs, and 11 RDRs candidates [73]. Sweet orange and pepper [74] also demonstrated diverse compositions with 13 AGOs, 5 DCLs, and 7 RDRs candidates, and 12 AGOs, 4 DCLs, and 6 RDRs candidates [75], respectively. Across these studies, AGOs emerged as the predominant RNAi-related gene family members, followed by RDRs, whereas DCLs typically constituted a minority. These findings underscore the critical roles and evolutionary variations of sRNA biogenesis genes in plants, highlighting their importance in RNA silencing pathways and adaptive responses to environmental challenges.

The chromosomal localization of the 28 Prupe-sRNA biogenesis genes revealed an uneven distribution across eight peach chromosomes. To analyze duplication patterns, we conducted phylogenetic analysis, identified functional domains and conserved motifs, and performed orthologous similarity assessments. Phylogenetic analysis indicated that PpAGOs segregate into three clades, a pattern consistent with earlier findings [19] and comparable to those observed in the Arabidopsis genome, suggesting highly conserved clade sizes between these two plant species. In our study, we identified a total of 97 AGOs, including 11 genes from the peach genome (*PpAGOs*), alongside counterparts from seven other Rosaceae species. Physicochemical analysis encompassed parameters such as isoelectric point (pI range: 8.5 to 9.8), molecular weight (MW range: 97.8 to 121.6), and sequence length (base pairs: 3498 to 9382) as well as protein length (amino acids: 872 to 1102) for each identified gene. Phylogenetic analysis of peach *AGO* genes delineated three primary clades. Notably, PpAGO8 and PpAGO9 were clustered with PpAGO4, while PpAGO4 itself clustered with three other genes (Prupe.2G056700, Prupe.2G056600, and Prupe.6G154800). Arabidopsis AGO3 did not align with any counterparts but clustered with AGO2, which in turn showed two PpAGO2 genes (Prupe.4G108100 and Prupe.4G108000). AGO1 was split into two duplicated PpAGO1 genes in our analysis. Additionally, the clades PpAGO5, PpAGO6, PpAGO7, and PpAGO10 each contained a single gene. Analysis of conserved functional motifs across peach and Arabidopsis revealed that the MID domain involved in sRNA-target interaction was conserved in all identified PpAGO proteins. Furthermore, PAZ, PIWI domain catalytic, H residue, and QF-V motifs were also identified. Chromoso-

mal mapping of *PpAGO* genes showed uneven distribution across six peach chromosomes, with chromosomes 7 and 8 lacking PpAGO gene members entirely. Also, in our study, we identified 77 RDRs across the genomes of eight Rosaceae species, analyzing their fundamental genomic characteristics and gene expression patterns. This represents the first comprehensive genome-wide analysis and evolutionary study of sRNA biogenesis, employing phylogenetic classifications, chromosomal locations, gene structure, and conserved motif analysis. Functional predictions were made by aligning conserved motifs, which were validated through gene regulation and RNA expression studies.

Drought stress not only affects root growth, but also affects plant growth and metabolism by preventing plant stomatal movement respiration, and photosynthesis in leaves [76]. To investigate the regulation of the RNA silencing pathway, we conducted experimental analysis of gene transcriptional changes in response to drought stress treatments. Gene expression was analyzed using FPKM values and quantitative qRT-PCR across different peach tissues. Our findings demonstrate dynamic regulation of RNA silencing, suggesting its potential involvement in coordinating peach development and environmental adaptation.

Moreover, the physiological and biochemical results including plant biomass, electrolyte leakage (EL), proline content, and total soluble sugar content showed that the Beijing 2-7 peach cultivar demonstrated resistance to drought stress as compared to the Sinai peach cultivar. This was consistent with our results of the gene expressions of the RNAi-related genes in both cultivars, which revealed that Beijing 2-7 was the tolerant cultivar compared with the Sinai cultivar, suggesting a strong relationship between these genes and drought resistance of peach trees.

The data presented offer valuable insights into the molecular evolution of AGO, DCL, and *RDR* genes within Rosaceae genomes, particularly in *P. persica*. This information enhances our understanding of how these mechanisms function to mitigate drought effects in plants. Additionally, it sheds light on the evolutionary history of these genes across various species within the Rosaceae family. This knowledge is pivotal for elucidating the adaptive strategies employed by peach and related species to cope with environmental stresses, contributing to broader agricultural and ecological applications. In summary, this study provides crucial insights into peach RNA silencing components, laying a foundation for selecting candidate factors and conducting detailed functional and mechanistic studies in the future.

4. Materials and Methods

4.1. Identification and Characterization of AGO, DCL, and RDR Genes in Rosaceae

The amino acid sequences of Arabidopsis *AGO*, *DCL*, and *RDR* genes were downloaded from the TAIR database (https://www.Arabidopsis.org/, accessed on 1 March 2023). Orthologous AGO, DCL, and RDR protein sequences from seven other Rosaceae species, including strawberry (*F. vesca*) [77], China rose (*R. chinensis*) [78,79], black raspberry (*R. occidentalis*) [80], apple (Malus × domestica) [81], pear (*P. communis*) [82], almond (*P. dulcis*) [83], and Armenian plum (*P. armeniaca*) [84], were retrieved from the GDR (http://www.rosaceae.org/, accessed on 7 March 2023) and Phytozome (https://phytozome-next.jgi.doe.gov/, accessed on 15 April 2023) databases [1,85]. The genome-wide prediction of peach *AGO*, *DCL*, and *RDR* genes was performed using HMMER 3.0 software (http://hmmer.janelia.org/, accessed on 11 March 2023) within the GDR platform. All identified *AGO*, *DCL*, and *RDR* genes were validated using the Conserved Domain Database (CDD) at the National Center for Biotechnology Information (NCBI) (https://www.ncbi.nlm.nih.gov/, accessed on 15 April 2023). Hidden Markov Models (HMM) and the Pfam protein family database (Pfam v3.1) [86] were employed to identify and annotate conserved domains within all protein sequences. The physicochemical properties of the identified peach *AGO*, *DCL*, and *RDR* genes, such as isoelectric point (*p*I), molecular weight (MW), and instability index, were calculated using Geneious Prime software 2024.0.5 [87]. The subcellular localization of the AGO, DCL, and RDR proteins was identified using the WoLF PSORT database (https://wolfpsort.hgc.jp/, accessed on 19 March 2023). A list of potential locations has

been detected using protein sequences. This investigation aimed to determine the most common location of the proteins within the cell [88].

4.2. Multiple Sequence Alignments and Phylogenetic Analysis of AGO, DCL and RDR Genes in Peach

The multiple sequence alignments of AGO, DCL, and RDR proteins from *P. persica* and Arabidopsis genomes were conducted using Clustal-W [89] within MEGA 11.0 software [75] with default parameters. The final sequences were validated and compiled using Geneious Prime software by comparing them against their respective homologs in the NCBI database. Subsequently, a neighbor-joining (NJ) phylogenetic tree [90] was constructed based on the protein sequences with 1000 bootstrap replicates [91] in MEGA to determine their evolutionary relationships. The evolutionary distances were computed using the Equal Input method [92].

4.3. Chromosomal Localization, Gene Structure, and Motif Analysis in Peach

The peach *AGO*, *DCL*, and *RDR* genes were positioned on the *P. persica* chromosomes using MapGene2 Chromosome V2 (http://mg2c.iask.in/mg2c_v2.0/, accessed on 23 March 2023) based on their genomic coordinates, and subsequently visualized using TBtools-II v2.102 [93]. For conserved motif analysis, known protein domains were identified using the SMART web server (http://smart.embl-heidelberg.de, accessed on 25 March 2023). Additionally, conserved motifs were predicted using the MEME web server (http://meme-suite.org/tools/meme, accessed on 28 March 2023) [94] with parameters set to an optimum motif width of $6 \leq n \leq 200$ and a maximum number of motifs of five. The identified motifs were annotated using Pfam [85,95].

4.4. Orthologous Similarity, Collinearity, and cis-Regulatory Elements Analysis for RNAi-Related Genes in Peach

The percentage similarity and identity between peach and Arabidopsis AGO, DCL, and RDR protein sequences were computed using the Ident and Sim online sequence manipulation tool (http://www.bioinformatics.org/sms2/ident_sim.html, accessed on 3 April 2023) [96]. Collinearity between the two genomes was assessed using MCScanX [97], with analyses conducted to identify segmental and tandem duplications that contribute to genome evolution. Synonymous (Ks) and nonsynonymous (Ka) substitution rates for homologous *AGO*, *DCL*, and *RDR* gene pairs were calculated using DnaSP v6.12.03 software [98]. The TBtools software [93] was utilized to visualize segmentally and tandemly duplicated genome regions. Additionally, *cis*-elements within the 2 kb regions upstream of *AGO*, *DCL*, and *RDR* genes were screened using PlantCARE (http://bioinformatics.psb.ugent.be/webtools/Plantcare/html/) (accessed on 10 April 2023) [99], and all results were visualized using TBtools.

4.5. Expression Analysis and qRT-PCR Validation

Short paired-end sequence reads of transcriptome data from the published Bioprojects PRJNA694331 and PRJNA694007 were utilized to assess the FPKM profiles of *AGO*, *DCL*, and *RDR* genes across various peach tissues (leaf, root, flowers, phloem, seeds, and fruits) under drought stress at different time points (0-, 6-, 12-, 24-, and 36-h, as well as 2-, 4-, 5-, 6-, 9-, 12-, and 14-days). Heatmaps visualizing the expression profiles of *AGO*, *DCL*, and *RDR* genes were generated using TBtools [93].

To validate the expression of these candidate genes under drought stress, two peach cultivars with contrasting drought tolerance levels were studied: the drought-resistant cultivar 'BJ2-7' and the drought-susceptible cultivar 'SN'. Seedlings of these cultivars were grown in a controlled environment for 3 months under specific light and temperature conditions with regular watering as previously described [100,101]. Subsequently, the seedlings were subjected to drought stress by withholding water for 14 days as previously described by [102–104], while the control plants were maintained under regular watering

conditions. Leaf (L) and root (R) samples were collected from each cultivar, immediately frozen in liquid nitrogen, and stored at −80 °C until RNA extraction.

To extract the total RNA, 100 mg of leaf and root tissues were used using the Magen RNA Extraction Kit (Magen Bio, Shanghai, China), treated with RNase-free DNase I (Promega, Madison, WI, USA) to eliminate genomic DNA contamination, and assessed for purity and concentration using a NanoDrop 2000 spectrophotometer (Thermo Scientific, Waltham, MA, USA). To synthesize the first-strand cDNA, 2 µg of total RNA was used using M-MLV reverse transcriptase (Promega, USA) according to the manufacturer's instructions.

Gene-specific primers for *AGO*, *DCL*, and *RDR* genes were designed based on NCBI sequences. All the primers used in this study are shown in Table S4. Quantitative real-time PCR (qRT-PCR) analysis was conducted using a qTOWER3.4 system (Analytik Jena, Jena, Germany) with Roche LightCycler480 SYBR Green I Master kits. The qRT-PCR reactions were performed in triplicate with biological replicates, and gene expression levels were normalized to the internal control gene *PpACTIN* (Prupe.8G132000) [105] using the $2^{-\Delta\Delta Ct}$ method [106].

4.6. Plants Physiological and Biochemical Evaluations

To evaluate the response of two peach cultivars to drought stress, plants were subjected to a 14-day drought treatment, with three plants randomly selected from each treatment (drought-stressed) and control group. The leaves and roots of selected plants were harvested. The roots were washed with distilled water and separated from the shoots. The fresh weights of the roots and shoots were measured using an analytical balance (precision 0.0001 g). After drying the shoots and roots in an oven at 80 °C for 24 h, their dry weights were measured to calculate total biomass as follows: Total fresh biomass (g) = shoot fresh weight + root fresh weight and Total dry biomass (g) = shoot dry weight + root dry weight.

Electrolyte leakage (EL) was assessed by collecting 0.5 g of fresh peach seedling leaves, which were washed three times with deionized water and transferred to 50 mL plastic centrifuge tubes with 15 mL of deionized water. After incubating for 12 h at room temperature on a conical shaker, initial conductivity (EL1) was measured using a JENCO-3173 conductivity meter (Jenco Instruments, Inc., San Diego, CA, USA). To release all electrolytes, leaves were autoclaved at 121 °C for 30 min, cooled, and the final conductivity (EL2) was measured. Relative EL was calculated as EL (%) = (EL1/EL2) × 100.

Sugar quantification (glucose, fructose, sucrose) was performed using High-performance Liquid Chromatography (HPLC; Shimadzu, Kyoto, Japan) coupled with a refractive index detector (RID-10 AL). The extraction involved sealing samples in plastic film and immersing them in boiling water for 30 min. Briefly, leaf and root samples were ground into powder in liquid nitrogen using an A11 Basic Analytical Mill (IKAWerke, Staufen, Germany) and approximately 0.5 g of powder was transferred to a clean Eppendorf tube. Soluble sugars were extracted with 6 mL deionized water by ultrasonic treatment for 15 min, and then centrifuged at 5000× *g* for 15 min. The resultant supernatant was filtered through a 0.22 µm Sep-Pak filter (ANPEL, Shanghai, China). Supernatants were collected twice, mixed, and analyzed after adding Anthrone reagent and sulfuric acid, followed by absorbance measurement at 620 nm to determine total soluble sugar concentration [107]. The injection volume was 20 µL, and chromatographic separation was performed using a CarboSep CHO-620 Ca column (300 mm × 6.5 mm, 10 µm particle size) and CarboSep CHO-620 Cartridge (Transgenomic, San Jose, CA, USA). The mobile phase was deionized water at the flow rate of 0.5 mL/min and the column temperature was maintained at 90 °C. The amount of soluble sugar concentration was obtained from the glucose standard curve [108,109].

Proline content was determined according to established methods using the acid ninhydrin test. Samples were processed using a standard proline curve, and proline concentrations were quantified to assess the stress response in peach cultivars under drought conditions.

4.7. Statistical Analysis

All experiments were conducted in three biological replicates. Analysis of' variance (ANOVA) was employed to analyze the data using Statistical Package for the Social Sciences (SPSS) software version 22.0 (IBM Corporation Chicago, IL, USA). All values are shown as mean + SD (n = 3). According to the experiments, the confidence levels of the statistically significant differences were analyzed using Duncan's test and Student's t-test. Origin 9.0 (Origin Lab, Inc., Hampton, MA, USA) and GraphPad Prism 9 (GraphPad Software, San Diego, CA, USA) were used to construct graphs.

Supplementary Materials: The following supporting information can be downloaded at: https://www.mdpi.com/article/10.3390/horticulturae10111228/s1, Figure S1. (A) Assessment of inter-domain accuracy for PpAGO6, highlighting expected position errors at residues when aligned with true structures, indicating high prediction reliability (AlphaFold). (B) Direct physical PPI fingerprint curves of Dicer protein homologs, distinguishing dimeric (blue) and tetrameric (green) quaternary structures critical for understanding molecular interactions and regulation, with differently colored boxes indicating motifs and their positions. (C) Assessment of inter-domain accuracy for PpRDR2, showing expected position errors at residues when aligned, indicative of robust prediction of domain positions (AlphaFold); Figure S2: *Cis*-elements in the 2 kb upstream region of the RNAi-related genes. A. *Cis*-elements for *PpAGO* B. *Cis*-elements for *PpDCL* C. *Cis*-elements for *PpRDR*. Different colors in the left lines indicate different types of *cis*-elements. The color intensity and number in the cells indicated the number of *cis*-element in these genes; Figure S3: Tissues and temporal FPKM expression trends (A, B). FPKM analysis of *PpDCL* genes in various peach tissues under drought stress. Left panels show high expression levels of *PpDCL* genes observed in peach seeds, fruits, roots, leaves, phloem, and flowers. Right panels depict temporal expression trends of *DCL* genes in the fruit flesh of *P. persica* exposed to drought stress over a 14-day period, with 0 h as the control. Expression profiles are categorized into three clusters (EC1, EC2, and EC3) based on standardized relative expression levels. RNA data were used to assess the expression of *PpDCL* genes; Table S1: Physicochemical characterization of Rosaceae *AGO* genes; Table S2: The detailed information of *DCL* genes among five Rosaceae genomes; Table S3: The RDR proteins profiles in seven Rosaceae species, Table S4: qRT-PCR primers used to validate the expression levels of *PpAGO*, *PpDCL*, *PpRDR* genes., Table S5: Preparation of proline standard curves.

Author Contributions: Conceptualization, M.B. and Y.C.; methodology, M.B., M.D.A.M. and M.M.; Software, M.B., M.M. and M.W.; resources, C.N.; validation, E.N. and C.S.; formal analysis, M.B. and M.W.; investigation, M.B. and M.E.; data curation, M.B., M.D.A.M. and C.O.; writing—original draft preparation, M.B., M.W. and C.O.; writing—review and editing, M.B., M.W., M.M., E.N. and W.Z.; visualization, M.B., M.M. and M.E.; supervision, E.N. and Y.H.; project administration and funding acquisition, Y.H. All authors have read and agreed to the published version of the manuscript.

Funding: This project was financially supported by the National Natural Science Foundation of China (U23A20206 and 32272687), the Key Special Project of Intergovernmental International Cooperation of the National Key R&D Program of China (2023YFE0125100), and the China Agriculture Research System (grant no. CARS-30).

Data Availability Statement: All data can be found online in the main text and supporting information materials. The RNA-seq data can be found in the Sequence Read Archive (SRA) database with accession numbers of PRJNA694007 and PRJNA694331.

Acknowledgments: We would like to appreciate the kind efforts of Heng Sun from the 'Aquatic Plant Research Center', Wuhan Botanical Garden, Chinese Academy of Sciences, and we appreciate the valuable efforts and his kind collaboration. Authors would like to thank Hubei Province Science and Technology Innovation Talent and Service Special International Science and Technology Cooperation Project (2022EHB045). In addition, authors would like to extend their thanks to Fundacion Seneca (Region de Murcia, Spain) for supporting M.M (Ref. 22416/SF/23).

Conflicts of Interest: The authors declare no conflicts of interest.

References

1. Verde, I.; Abbott, A.G.; Scalabrin, S.; Jung, S.; Shu, S.; Marroni, F.; Zhebentyayeva, T.; Dettori, M.T.; Grimwood, J.; Cattonaro, F.; et al. The high-quality draft genome of peach (*Prunus persica*) identifies unique patterns of genetic diversity, domestication and genome evolution. *Nat. Genet.* **2013**, *45*, 487–494. [CrossRef] [PubMed]
2. Cao, K.; Zheng, Z.; Wang, L.; Liu, X.; Zhu, G.; Fang, W.; Cheng, S.; Zeng, P.; Chen, C.; Wang, X. Comparative population genomics reveals the domestication history of the peach, *Prunus persica*, and human influences on perennial fruit crops. *Genome Biol.* **2014**, *15*, 415. [CrossRef] [PubMed]
3. Byrne, D.H.; Raseira, M.B.; Bassi, D.; Piagnani, M.C.; Gasic, K.; Reighard, G.L.; Moreno, M.A.; Pérez, S. Peach. In *Fruit Breeding*; Springer: Boston, MA, USA, 2012; pp. 505–569.
4. Arús, P.; Verde, I.; Sosinski, B.; Zhebentyayeva, T.; Abbott, A.G. The peach genome. *Tree Genet. Genomes* **2012**, *8*, 531–547. [CrossRef]
5. Rahmati, M.; Vercambre, G.; Davarynejad, G.; Bannayan, M.; Azizi, M.; Genard, M. Water scarcity conditions affect peach fruit size and polyphenol contents more severely than other fruit quality traits. *J. Sci. Food Agric.* **2014**, *95*, 1055–1065. [CrossRef] [PubMed]
6. Haider, M.S.; Kurjogi, M.M.; Khalil-ur-Rehman, M.; Pervez, T.; Songtao, J.; Fiaz, M.; Jogaiah, S.; Wang, C.; Fang, J. Drought stress revealed physiological, biochemical and gene-expressional variations in 'Yoshihime' peach (*Prunus persica* L.) cultivar. *J. Plant Interact.* **2018**, *13*, 83–90. [CrossRef]
7. Belal, M.A.; El-Alakmy, H.A.; Abdelhameed, A.A.; Sourour, M.M. Influence of reducing irrigation rate and addition of super absorbent polymer on peach trees growth under north sinai conditions. *Sinai J. Appl. Sci.* **2017**, *6*, 249–258. [CrossRef]
8. Usman, M.; Bokhari, S.A.M.; Fatima, B.; Rashid, B.; Nadeem, F.; Sarwar, M.B.; Nawaz-ul-Rehman, M.S.; Shahid, M.; Ayub, C.M. Drought stress mitigating morphological, physiological, biochemical, and molecular responses of guava (*Psidium guajava* L.) cultivars. *Front. Plant Sci.* **2022**, *13*, 878616. [CrossRef]
9. Wang, Z.; Ni, L.; Hua, J.; Liu, L.; Yin, Y.; Li, H.; Gu, C. Transcriptome analysis reveals regulatory framework for salt and drought tolerance in *Hibiscus hamabo* siebold & zuccarini. *Forests* **2021**, *12*, 454. [CrossRef]
10. Talebizadeh, Z. Regulation of Gene Expression by Small RNAs. *Am. J. Hum. Genet.* **2010**, *86*, 328–330. [CrossRef]
11. Hutvágner, G.; Zamore, P.D. RNAi: Nature abhors a double-strand. *Curr. Opin. Genet. Dev.* **2002**, *12*, 225–232. [CrossRef]
12. Fang, X.; Qi, Y. RNAi in plants: An argonaute-centered view. *Plant Cell* **2016**, *28*, 272–285. [CrossRef] [PubMed]
13. Khare, T.; Shriram, V.; Kumar, V. RNAi technology: The role in development of abiotic stress-tolerant crops. In *Biochemical, Physiological and Molecular Avenues for Combating Abiotic Stress Tolerance in Plants*; Elsevier: Amsterdam, The Netherlands, 2018; pp. 117–133.
14. Bai, M.; Yang, G.S.; Chen, W.T.; Mao, Z.C.; Kang, H.X.; Chen, G.H.; Yang, Y.H.; Xie, B.Y. Genome-wide identification of Dicer-like, Argonaute and RNA-dependent RNA polymerase gene families and their expression analyses in response to viral infection and abiotic stresses in *Solanum lycopersicum*. *Gene* **2012**, *501*, 52–62. [CrossRef] [PubMed]
15. Borges, F.; Martienssen, R.A. The expanding world of small RNAs in plants. *Nat. Rev. Mol. Cell Biol.* **2015**, *16*, 727–741. [CrossRef] [PubMed]
16. Noronha Fernandes-Brum, C.; Marinho Rezende, P.; Cherubino Ribeiro, T.H.; Ricon de Oliveira, R.; Cunha de Sousa Cardoso, T.; Rodrigues do Amaral, L.; de Souza Gomes, M.; Chalfun-Junior, A. A genome-wide analysis of the RNA-guided silencing pathway in coffee reveals insights into its regulatory mechanisms. *PLoS ONE* **2017**, *12*, e0176333. [CrossRef]
17. Ruiz-Ferrer, V.; Voinnet, O. Roles of plant small RNAs in biotic stress responses. *Annu. Rev. Plant Biol.* **2009**, *60*, 485–510. [CrossRef]
18. Das, S.; Swetha, C.; Pachamuthu, K.; Nair, A.; Shivaprasad, P.V. Loss of function of Oryza sativa Argonaute 18 induces male sterility and reduction in phased small RNAs. *Plant Reprod.* **2020**, *33*, 59–73. [CrossRef]
19. Li, Z.; Li, W.; Guo, M.; Liu, S.; Liu, L.; Yu, Y.; Mo, B.; Chen, X.; Gao, L. Origin, evolution and diversification of plant ARGONAUTE proteins. *Plant J.* **2022**, *109*, 1086–1097. [CrossRef]
20. Gelaw, T.A.; Sanan-Mishra, N. Non-coding RNAs in response to drought stress. *Int. J. Mol. Sci.* **2021**, *22*, 12519. [CrossRef] [PubMed]
21. Budak, H.; Zhang, B. *MicroRNAs in Model and Complex Organisms*; Springer: Berlin/Heidelberg, Germany, 2017; Volume 17, pp. 121–124.
22. Tiwari, R.; Rajam, M.V. RNA-and miRNA-interference to enhance abiotic stress tolerance in plants. *J. Plant Biochem. Biotechnol.* **2022**, *31*, 689–704. [CrossRef]
23. Saplaoura, E.; Kragler, F. Mobile Transcripts and Intercellular Communication in Plants. *Enzymes* **2016**, *40*, 1–29. [CrossRef]
24. Kehr, J.; Kragler, F. Long distance RNA movement. *New Phytol.* **2018**, *218*, 29–40. [CrossRef] [PubMed]
25. Schaefer, M.; Nabih, A.; Spies, D.; Hermes, V.; Bodak, M.; Wischnewski, H.; Stalder, P.; Ngondo, R.P.; Liechti, L.A.; Sajic, T.; et al. Global and precise identification of functional miRNA targets in mESCs by integrative analysis. *EMBO Rep.* **2022**, *23*, e54762. [CrossRef] [PubMed]
26. Sokolowska, A.; Rugala, M.; Oracz, K. ARGONAUTE proteins in cell biology and plant development. *Postepy Biochem.* **2022**, *68*, 310–320. [CrossRef]
27. Vaucheret, H. Post-transcriptional small RNA pathways in plants: Mechanisms and regulations. *Genes Dev.* **2006**, *20*, 759–771. [CrossRef]

28. Chapman, E.J.; Carrington, J.C. Specialization and evolution of endogenous small RNA pathways. *Nat. Rev. Genet.* **2007**, *8*, 884–896. [CrossRef] [PubMed]
29. Kapoor, M.; Arora, R.; Lama, T.; Nijhawan, A.; Khurana, J.P.; Tyagi, A.K.; Kapoor, S. Genome-wide identification, organization and phylogenetic analysis of Dicer-like, Argonaute and RNA-dependent RNA Polymerase gene families and their expression analysis during reproductive development and stress in rice. *BMC Genom.* **2008**, *9*, 451. [CrossRef]
30. Qu, F.; Ye, X.; Morris, T.J. Arabidopsis DRB4, AGO1, AGO7, and RDR6 participate in a DCL4-initiated antiviral RNA silencing pathway negatively regulated by DCL1. *Proc. Natl. Acad. Sci. USA* **2008**, *105*, 14732–14737. [CrossRef]
31. Cao, Y.; Xu, X.; Jiang, L. Integrative analysis of the RNA interference toolbox in two Salicaceae willow species, and their roles in stress response in poplar (*Populus trichocarpa* Torr. & Gray). *Int. J. Biol. Macromol.* **2020**, *162*, 1127–1139. [CrossRef]
32. Balassa, G.; Balassa, K.; Janda, T.; Rudnóy, S. Expression Pattern of RNA Interference Genes During Drought Stressand MDMV Infection in Maize. *J. Plant Growth Regul.* **2022**, *41*, 2048–2058. [CrossRef]
33. Chen, W.; Choi, J.; Li, X.; Nathans, J.F.; Martin, B.; Yang, W.; Hamazaki, N.; Qiu, C.; Lalanne, J.-B.; Regalado, S. Symbolic recording of signalling and cis-regulatory element activity to DNA. *Nature* **2024**, *632*, 1073–1081. [CrossRef]
34. Marand, A.P.; Eveland, A.L.; Kaufmann, K.; Springer, N.M. cis-Regulatory elements in plant development, adaptation, and evolution. *Annu. Rev. Plant Biol.* **2023**, *74*, 111–137. [CrossRef] [PubMed]
35. Belal, M.A.; Ezzat, M.; Zhang, Y.; Xu, Z.; Cao, Y.; Han, Y. Integrative Analysis of the DICER-like (DCL) Genes from Peach (*Prunus persica*): A Critical Role in Response to Drought Stress. *Front. Ecol. Evol.* **2022**, *10*, 923166. [CrossRef]
36. Ahmed, F.F.; Hossen, M.I.; Sarkar, M.A.R.; Konak, J.N.; Zohra, F.T.; Shoyeb, M.; Mondal, S. Genome-wide identification of DCL, AGO and RDR gene families and their associated functional regulatory elements analyses in banana (*Musa acuminata*). *PLoS ONE* **2021**, *16*, e0256873. [CrossRef] [PubMed]
37. Wang, J.; Wang, Z.; Jia, C.; Miao, H.; Zhang, J.; Liu, J.; Xu, B.; Jin, Z. Genome-wide identification and transcript analysis of TCP gene family in Banana (*Musa acuminata* L.). *Biochem. Genet.* **2022**, *60*, 204–222. [CrossRef] [PubMed]
38. Parker, J.S.; Barford, D. Argonaute: A scaffold for the function of short regulatory RNAs. *Trends Biochem. Sci.* **2006**, *31*, 622–630. [CrossRef]
39. Vaucheret, H. Plant argonautes. *Trends Plant Sci.* **2008**, *13*, 350–358. [CrossRef]
40. Hamar, E.; Szaker, H.M.; Kis, A.; Dalmadi, A.; Miloro, F.; Szittya, G.; Taller, J.; Gyula, P.; Csorba, T.; Havelda, Z. Genome-Wide Identification of RNA Silencing-Related Genes and Their Expressional Analysis in Response to Heat Stress in Barley (*Hordeum vulgare* L.). *Biomolecules* **2020**, *10*, 929. [CrossRef]
41. Hutvagner, G.; Simard, M.J. Argonaute proteins: Key players in RNA silencing. *Nat. Rev. Mol. Cell Biol.* **2008**, *9*, 22–32. [CrossRef]
42. Kwak, P.B.; Tomari, Y. The N domain of Argonaute drives duplex unwinding during RISC assembly. *Nat. Struct. Mol. Biol.* **2012**, *19*, 145–151. [CrossRef]
43. Arribas-Hernández, L.; Marchais, A.; Poulsen, C.; Haase, B.; Hauptmann, J.; Benes, V.; Meister, G.; Brodersen, P. The slicer activity of ARGONAUTE1 is required specifically for the phasing, not production, of trans-acting short interfering RNAs in Arabidopsis. *Plant Cell* **2016**, *28*, 1563–1580. [CrossRef]
44. Cerutti, L.; Mian, N.; Bateman, A. Domains in gene silencing and cell differentiation proteins: The novel PAZ domain and redefinition of the Piwi domain. *Trends Biochem. Sci.* **2000**, *25*, 481–482. [CrossRef] [PubMed]
45. Jinek, M.; Doudna, J.A. A three-dimensional view of the molecular machinery of RNA interference. *Nature* **2009**, *457*, 405–412. [CrossRef] [PubMed]
46. Moazed, D. Small RNAs in transcriptional gene silencing and genome defence. *Nature* **2009**, *457*, 413–420. [CrossRef] [PubMed]
47. Simon, B.; Kirkpatrick, J.P.; Eckhardt, S.; Reuter, M.; Rocha, E.A.; Andrade-Navarro, M.A.; Sehr, P.; Pillai, R.S.; Carlomagno, T. Recognition of 2′-O-methylated 3′-end of piRNA by the PAZ domain of a Piwi protein. *Structure* **2011**, *19*, 172–180. [CrossRef]
48. Rivas, F.V.; Tolia, N.H.; Song, J.-J.; Aragon, J.P.; Liu, J.; Hannon, G.J.; Joshua-Tor, L. Purified Argonaute2 and an siRNA form recombinant human RISC. *Nat. Struct. Mol. Biol.* **2005**, *12*, 340–349. [CrossRef]
49. Höck, J.; Meister, G. The Argonaute protein family. *Genome Biol.* **2008**, *9*, 210. [CrossRef] [PubMed]
50. Mi, S.; Cai, T.; Hu, Y.; Chen, Y.; Hodges, E.; Ni, F.; Wu, L.; Li, S.; Zhou, H.; Long, C. Sorting of small RNAs into Arabidopsis argonaute complexes is directed by the 5′ terminal nucleotide. *Cell* **2008**, *133*, 116–127. [CrossRef]
51. Frank, F.; Hauver, J.; Sonenberg, N.; Nagar, B. Arabidopsis Argonaute MID domains use their nucleotide specificity loop to sort small RNAs. *EMBO J.* **2012**, *31*, 3588–3595. [CrossRef]
52. Thieme, C.J.; Schudoma, C.; May, P.; Walther, D. Give it AGO: The search for miRNA-Argonaute sorting signals in *Arabidopsis thaliana* indicates a relevance of sequence positions other than the 5′-position alone. *Front. Plant Sci.* **2012**, *3*, 272. [CrossRef]
53. Niaz, S. The AGO proteins: An overview. *Biol. Chem.* **2018**, *399*, 525–547. [CrossRef]
54. Bernstein, E.; Caudy, A.A.; Hammond, S.M.; Hannon, G.J. Role for a bidentate ribonuclease in the initiation step of RNA interference. *Nature* **2001**, *409*, 363–366. [CrossRef] [PubMed]
55. Zhang, H.; Kolb, F.A.; Jaskiewicz, L.; Westhof, E.; Filipowicz, W. Single processing center models for human Dicer and bacterial RNase III. *Cell* **2004**, *118*, 57–68. [CrossRef] [PubMed]
56. Wei, X.; Ke, H.; Wen, A.; Gao, B.; Shi, J.; Feng, Y. Structural basis of microRNA processing by Dicer-like 1. *Nat. Plants* **2021**, *7*, 1389–1396. [CrossRef] [PubMed]
57. Wang, Y.-X.; Liu, Z.-W.; Wu, Z.-J.; Li, H.; Wang, W.-L.; Cui, X.; Zhuang, J. Genome-wide identification and expression analysis of GRAS family transcription factors in tea plant (*Camellia sinensis*). *Sci. Rep.* **2018**, *8*, 3949. [CrossRef] [PubMed]

58. Baumberger, N.; Baulcombe, D. Arabidopsis ARGONAUTE1 is an RNA Slicer that selectively recruits microRNAs and short interfering RNAs. *Proc. Natl. Acad. Sci. USA* **2005**, *102*, 11928–11933. [CrossRef]
59. Vaucheret, H.; Vazquez, F.; Crété, P.; Bartel, D.P. The action of ARGONAUTE1 in the miRNA pathway and its regulation by the miRNA pathway are crucial for plant development. *Genes Dev.* **2004**, *18*, 1187–1197. [CrossRef]
60. Banerjee, J.; Sahoo, D.K.; Dey, N.; Houtz, R.L.; Maiti, I.B. An intergenic region shared by At4g35985 and At4g35987 in Arabidopsis thaliana is a tissue specific and stress inducible bidirectional promoter analyzed in transgenic *Arabidopsis* and tobacco plants. *PLoS ONE* **2013**, *8*, e79622. [CrossRef]
61. Younger, P. Stedman's Medical Dictionary. *Ref. Rev.* **2007**, *21*, 41–42.
62. Mainz, D.; Quadt, I.; Stranzenbach, A.K.; Voss, D.; Guarino, L.A.; Knebel-Mörsdorf, D. Expression and nuclear localization of the TATA-box-binding protein during baculovirus infection. *J. Gen. Virol.* **2014**, *95*, 1396–1407. [CrossRef]
63. Howell, M.D.; Fahlgren, N.; Chapman, E.J.; Cumbie, J.S.; Sullivan, C.M.; Givan, S.A.; Kasschau, K.D.; Carrington, J.C. Genome-wide analysis of the RNA-DEPENDENT RNA POLYMERASE6/DICER-LIKE4 pathway in Arabidopsis reveals dependency on miRNA- and tasiRNA-directed targeting. *Plant Cell* **2007**, *19*, 926–942. [CrossRef]
64. Garcia-Ruiz, H.; Takeda, A.; Chapman, E.J.; Sullivan, C.M.; Fahlgren, N.; Brempelis, K.J.; Carrington, J.C. Arabidopsis RNA-dependent RNA polymerases and dicer-like proteins in antiviral defense and small interfering RNA biogenesis during Turnip Mosaic Virus infection. *Plant Cell* **2010**, *22*, 481–496. [CrossRef] [PubMed]
65. Martínez de Alba, A.E.; Moreno, A.B.; Gabriel, M.; Mallory, A.C.; Christ, A.; Bounon, R.; Balzergue, S.; Aubourg, S.; Gautheret, D.; Crespi, M.D. In plants, decapping prevents RDR6-dependent production of small interfering RNAs from endogenous mRNAs. *Nucleic Acids Res.* **2015**, *43*, 2902–2913. [CrossRef] [PubMed]
66. Polydore, S.; Axtell, M.J. Analysis of RDR1/RDR2/RDR6-independent small RNAs in Arabidopsis thaliana improves MIRNA annotations and reveals unexplained types of short interfering RNA loci. *Plant J.* **2018**, *94*, 1051–1063. [CrossRef] [PubMed]
67. Yan, Y.; Ham, B.K. The Mobile Small RNAs: Important Messengers for Long-Distance Communication in Plants. *Front. Plant Sci.* **2022**, *13*, 928729. [CrossRef]
68. Song, L.; Fang, Y.; Chen, L.; Wang, J.; Chen, X. Role of non-coding RNAs in plant immunity. *Plant Commun.* **2021**, *2*, 100180. [CrossRef]
69. Brant, E.J.; Budak, H. Plant small non-coding RNAs and their roles in biotic stresses. *Front. Plant Sci.* **2018**, *9*, 1038. [CrossRef]
70. Jing, X.; Xu, L.; Huai, X.; Zhang, H.; Zhao, F.; Qiao, Y. Genome-Wide Identification and Characterization of Argonaute, Dicer-like and RNA-Dependent RNA Polymerase Gene Families and Their Expression Analyses in *Fragaria* spp. *Genes* **2023**, *14*, 121. [CrossRef]
71. Krishnatreya, D.B.; Baruah, P.M.; Dowarah, B.; Chowrasia, S.; Mondal, T.K.; Agarwala, N. Genome-wide identification, evolutionary relationship and expression analysis of AGO, DCL and RDR family genes in tea. *Sci. Rep.* **2021**, *11*, 8679. [CrossRef]
72. Cui, D.L.; Meng, J.Y.; Ren, X.Y.; Yue, J.J.; Fu, H.Y.; Huang, M.T.; Zhang, Q.Q.; Gao, S.J. Genome-wide identification and characterization of DCL, AGO and RDR gene families in *Saccharum spontaneum*. *Sci. Rep.* **2020**, *10*, 13202. [CrossRef]
73. Sabbione, A.; Daurelio, L.; Vegetti, A.; Talon, M.; Tadeo, F.; Dotto, M. Genome-wide analysis of AGO, DCL and RDR gene families reveals RNA-directed DNA methylation is involved in fruit abscission in *Citrus sinensis*. *BMC Plant Biol.* **2019**, *19*, 401. [CrossRef]
74. Qin, L.; Mo, N.; Muhammad, T.; Liang, Y. Genome-Wide Analysis of DCL, AGO, and RDR Gene Families in Pepper (*Capsicum annuum* L.). *Int. J. Mol. Sci.* **2018**, *19*, 1038. [CrossRef] [PubMed]
75. Tamura, K.; Stecher, G.; Kumar, S. MEGA11: Molecular evolutionary genetics analysis version 11. *Mol. Biol. Evol.* **2021**, *38*, 3022–3027. [CrossRef] [PubMed]
76. Yang, X.; Lu, M.; Wang, Y.; Wang, Y.; Liu, Z.; Chen, S. Response Mechanism of Plants to Drought Stress. *Horticulturae* **2021**, *7*, 50. [CrossRef]
77. Folta, K.M.; Davis, T.M. Strawberry genes and genomics. *Crit. Rev. Plant Sci.* **2006**, *25*, 399–415. [CrossRef]
78. Lin, W.; Huang, J.; Xue, M.; Wang, X.; Wang, C. Characterization of the complete chloroplast genome of Chinese rose, *Rosa chinensis* (Rosaceae: Rosa). *Mitochondrial DNA Part B* **2019**, *4*, 2984–2985. [CrossRef]
79. Hibrand Saint-Oyant, L.; Ruttink, T.; Hamama, L.; Kirov, I.; Lakhwani, D.; Zhou, N.-N.; Bourke, P.; Daccord, N.; Leus, L.; Schulz, D. A high-quality genome sequence of *Rosa chinensis* to elucidate ornamental traits. *Nat. Plants* **2018**, *4*, 473–484. [CrossRef]
80. VanBuren, R.; Wai, C.M.; Colle, M.; Wang, J.; Sullivan, S.; Bushakra, J.M.; Liachko, I.; Vining, K.J.; Dossett, M.; Finn, C.E.; et al. A near complete, chromosome-scale assembly of the black raspberry (*Rubus occidentalis*) genome. *Gigascience* **2018**, *7*, giy094. [CrossRef]
81. Bianco, L.; Cestaro, A.; Sargent, D.J.; Banchi, E.; Derdak, S.; Di Guardo, M.; Salvi, S.; Jansen, J.; Viola, R.; Gut, I.; et al. Development and validation of a 20 K single nucleotide polymorphism (SNP) whole genome genotyping array for apple (*Malus* × *domestica* Borkh). *PLoS ONE* **2014**, *9*, e110377. [CrossRef]
82. Qiao, X.; Li, M.; Li, L.; Yin, H.; Wu, J.; Zhang, S. Genome-wide identification and comparative analysis of the heat shock transcription factor family in Chinese white pear (*Pyrus bretschneideri*) and five other *Rosaceae* species. *BMC Plant Biol.* **2015**, *15*, 12. [CrossRef]
83. Alioto, T.; Alexiou, K.G.; Bardil, A.; Barteri, F.; Castanera, R.; Cruz, F.; Dhingra, A.; Duval, H.; Fernandez, I.M.A.; Frias, L.; et al. Transposons played a major role in the diversification between the closely related almond and peach genomes: Results from the almond genome sequence. *Plant J.* **2020**, *101*, 455–472. [CrossRef]

84. Jiang, F.; Zhang, J.; Wang, S.; Yang, L.; Luo, Y.; Gao, S.; Zhang, M.; Wu, S.; Hu, S.; Sun, H.; et al. The apricot (*Prunus armeniaca* L.) genome elucidates Rosaceae evolution and beta-carotenoid synthesis. *Hortic. Res.* **2019**, *6*, 128. [CrossRef] [PubMed]
85. Goodstein, D.M.; Shu, S.; Howson, R.; Neupane, R.; Hayes, R.D.; Fazo, J.; Mitros, T.; Dirks, W.; Hellsten, U.; Putnam, N. Phytozome: A comparative platform for green plant genomics. *Nucleic Acids Res.* **2012**, *40*, D1178–D1186. [CrossRef] [PubMed]
86. Finn, R.D.; Bateman, A.; Clements, J.; Coggill, P.; Eberhardt, R.Y.; Eddy, S.R.; Heger, A.; Hetherington, K.; Holm, L.; Mistry, J. Pfam: The protein families database. *Nucleic Acids Res.* **2014**, *42*, D222–D230. [CrossRef] [PubMed]
87. Kearse, M.; Moir, R.; Wilson, A.; Stones-Havas, S.; Cheung, M.; Sturrock, S.; Buxton, S.; Cooper, A.; Markowitz, S.; Duran, C. Geneious Basic: An integrated and extendable desktop software platform for the organization and analysis of sequence data. *Bioinformatics* **2012**, *28*, 1647–1649. [CrossRef]
88. Kavas, M.; Mostafa, K.; Seçgin, Z.; Yerlikaya, B.A.; Yıldırım, K.; Gökdemir, G. Genome-wide analysis of DUF221 domain-containing gene family in common bean and identification of its role on abiotic and phytohormone stress response. *Genet. Resour. Crop Evol.* **2022**, *70*, 169–188. [CrossRef]
89. Thompson, J.D.; Higgins, D.G.; Gibson, T.J. CLUSTAL W: Improving the sensitivity of progressive multiple sequence alignment through sequence weighting, position-specific gap penalties and weight matrix choice. *Nucleic Acids Res.* **1994**, *22*, 4673–4680. [CrossRef] [PubMed]
90. Saitou, N.; Nei, M. The neighbor-joining method: A new method for reconstructing phylogenetic trees. *Mol. Biol. Evol.* **1987**, *4*, 406–425.
91. Felsenstein, J. Confidence limits on phylogenies: An approach using the bootstrap. *Evolution* **1985**, *39*, 783–791. [CrossRef]
92. Tajima, F.; Nei, M. Estimation of evolutionary distance between nucleotide sequences. *Mol. Biol. Evol.* **1984**, *1*, 269–285.
93. Chen, C.; Chen, H.; Zhang, Y.; Thomas, H.R.; Frank, M.H.; He, Y.; Xia, R. TBtools: An integrative toolkit developed for interactive analyses of big biological data. *Mol. Plant* **2020**, *13*, 1194–1202. [CrossRef]
94. Bailey, T.L.; Johnson, J.; Grant, C.E.; Noble, W.S. The MEME suite. *Nucleic Acids Res.* **2015**, *43*, W39–W49. [CrossRef] [PubMed]
95. Bateman, A.; Birney, E.; Durbin, R.; Eddy, S.R.; Finn, R.D.; Sonnhammer, E.L. Pfam 3.1: 1313 multiple alignments and profile HMMs match the majority of proteins. *Nucleic Acids Res.* **1999**, *27*, 260–262. [CrossRef] [PubMed]
96. Stothard, P. The sequence manipulation suite: JavaScript programs for analyzing and formatting protein and DNA sequences. *Biotechniques* **2000**, *28*, 1102–1104. [CrossRef]
97. Wang, Y.; Tang, H.; Debarry, J.D.; Tan, X.; Li, J.; Wang, X.; Lee, T.-H.; Jin, H.; Marler, B.; Guo, H. MCScanX: A toolkit for detection and evolutionary analysis of gene synteny and collinearity. *Nucleic Acids Res.* **2012**, *40*, e49. [CrossRef]
98. Rozas, J.; Ferrer-Mata, A.; Sánchez-DelBarrio, J.C.; Guirao-Rico, S.; Librado, P.; Ramos-Onsins, S.E.; Sánchez-Gracia, A. DnaSP 6: DNA sequence polymorphism analysis of large data sets. *Mol. Biol. Evol.* **2017**, *34*, 3299–3302. [CrossRef]
99. Rombauts, S.; Déhais, P.; Van Montagu, M.; Rouzé, P. PlantCARE, a plant cis-acting regulatory element database. *Nucleic Acids Res.* **1999**, *27*, 295–296. [CrossRef]
100. Gao, H.; Yu, W.; Yang, X.; Liang, J.; Sun, X.; Sun, M.; Xiao, Y.; Peng, F. Silicon enhances the drought resistance of peach seedlings by regulating hormone, amino acid, and sugar metabolism. *BMC Plant Biol.* **2022**, *22*, 422. [CrossRef] [PubMed]
101. Rieger, M. Growth, gas exchange, water uptake, and drought response of seedling-and cutting-propagated peach and citrus rootstocks. *J. Am. Soc. Hortic. Sci.* **1992**, *117*, 834–840. [CrossRef]
102. Lo Bianco, R.; Rieger, M.; Sung, S.J.S. Effect of drought on sorbitol and sucrose metabolism in sinks and sources of peach. *Physiol. Plant.* **2000**, *108*, 71–78. [CrossRef]
103. Goldhammer, D.; Salinas, M.; Crisosto, C.; Day, K.; Soler, M.; Moriana, A. Effects of regulated deficit irrigation and partial root zone drying on late harvest peach tree performance. In Proceedings of the V International Peach Symposium 592, Davis, CA, USA, 8–11 July 2001.
104. Jiménez, S.; Dridi, J.; Gutiérrez, D.; Moret, D.; Irigoyen, J.J.; Moreno, M.A.; Gogorcena, Y. Physiological, biochemical and molecular responses in four *Prunus rootstocks* submitted to drought stress. *Tree Physiol.* **2013**, *33*, 1061–1075. [CrossRef]
105. Wang, L.; Wei, J.; Shi, X.; Qian, W.; Mehmood, J.; Yin, Y.; Jia, H. Identification of the Light-Harvesting Chlorophyll a/b Binding Protein Gene Family in Peach (*Prunus persica* L.) and Their Expression under Drought Stress. *Genes* **2023**, *14*, 1475. [CrossRef] [PubMed]
106. Livak, K.J.; Schmittgen, T.D. Analysis of relative gene expression data using real-time quantitative PCR and the $2^{-\Delta\Delta CT}$ method. *Methods* **2001**, *25*, 402–408. [CrossRef] [PubMed]
107. Zill, L. Anthrone reagent. *Anal. Chem.* **1956**, *28*, 1577–1580. [CrossRef]
108. Tihomirova, K.; Dalecka, B.; Mezule, L. Application of conventional HPLC RI technique for sugar analysis in hydrolysed hay. *Agron. Res.* **2016**, *14*, 1713–1719.
109. Wassie, M.; Zhang, W.; Zhang, Q.; Ji, K.; Cao, L.; Chen, L. Exogenous salicylic acid ameliorates heat stress-induced damages and improves growth and photosynthetic efficiency in alfalfa (*Medicago sativa* L.). *Ecotoxicol. Environ. Saf.* **2020**, *191*, 110206. [CrossRef]